이학석사 학위논문

# Diagrammatic approach to dc conductivity in anisotropic disordered systems

무질서한 비등방성계에서의 직류 전도도에 대한
다이어그램 접근법

2020년 8월

서울대학교 대학원
물리천문학부
김 성 훈

이학석사 학위논문

# Diagrammatic approach to dc conductivity in anisotropic disordered systems

무질서한 비등방성계에서의 직류 전도도에 대한
다이어그램 접근법

2020년 8월

서울대학교 대학원
물리천문학부
김 성 훈

# Diagrammatic approach to dc conductivity in anisotropic disordered systems

무질서한 비등방성계에서의 직류 전도도에 대한
다이어그램 접근법


지도교수 민 홍 기


이 논문을 이학석사 학위논문으로 제출함

2020년 8월


서울대학교 대학원

물리천문학부

김 성 훈


김성훈의 이학석사 학위 논문을 인준함

2020년 8월


위 원 장: _____

부위원장: _____

위    원: _____

# Abstract

Transport in disordered systems is one of central themes in condensed matter physics. For systems with an isotropic energy dispersion, various theoretical approaches, including the Boltzmann transport theory and the Kubo formula, have provided us with useful frameworks for studying transport in disordered systems. Notably, it turns out that the two approaches give the consistent correction to dc conductivity in isotropic systems.

However, it has been elusive to correctly compute transport properties of systems with an arbitrarily anisotropic Fermi surface, especially by using a diagrammatic approach. Motivated by this point, this thesis is devoted to the development of a diagrammatic formalism for computing the dc conductivity of anisotropic systems.

We start by developing a generalized theory of transport in the semiclassical regime (i.e. $k_{\mathrm{F}}\ell_e \gg 1$), in the presence of electron-impurity and electron-phonon scatterings, respectively. First, we brief on the semiclassical Boltzmann approach in anisotropic multiband systems. Next, using the Kubo formula, we study the ladder approximation in anisotropic multiband systems and derive a relation satisfied by the transport relaxation time. As a result, we verify that the two theories are generally equivalent.

Then we turn to a unique transport feature in the quantum regime (i.e. $k_{\mathrm{F}}\ell_e \sim 1$), so-called weak localization. We rewrite the Bethe-Salepter equation and derive a Cooperon ansatz, which captures the anisotropy and Berry phase of the system. Using this ansatz, we develop a systematic quantum interference theory and apply it to various phases of few-layer black phosphorus. As a result, we predict that the magnetoconductivity at the semi-Dirac transition point will exhibit a nontrivial power-law dependence on the magnetic field, while following the conventional logarithmic field dependence of two-dimensional systems in the insulator and Dirac semimetal phases. Notably, the ratio between the magnetoconductivity and Boltzmann conductivity turns

out to be independent of the direction, even in strongly anisotropic systems.

# Contents

# List of Figures

# Chapter 1

# Introduction

Transport properties of disordered systems have been subjects of intense study in condensed matter physics [1–3]. They can be significantly altered depending on several characteristic lengths of the system, including the de-Broglie wavelength and the mean-free path [4, 5]. In weakly interacting systems, an electron can be interpreted as a quasiparticle that suffers collisions at a finite time interval, which is referred to as the relaxation time. The relevant characteristic length is the mean-free path, $\ell_e$, which characterizes the distance that the electron travels between two successive collisions. When the de-Broglie wavelength is much smaller than the mean-free path (i.e. $k_F \ell_e \gg 1$), electrons can be viewed as semiclassical particles. In contrast, when the two characteristic lengths are comparable (i.e. $k_F \ell_e \sim 1$), electrons should be regarded as quantum particles, which can exhibit interference phenomena. Thus, one should expect that distinct transport features would be found in each regime.

In the semiclassical regime, the Boltzmann transport theory within the relaxation time approximation is known to be valid. For an isotropic single-band system, the transport relaxation time $\tau_{\boldsymbol{k}}^{\mathrm{tr}}$ at state $\boldsymbol{k}$ in the relaxation time approximation is given by [6]

$$\frac{1}{\tau_{\boldsymbol{k}}^{\mathrm{tr}}} = \int \frac{d^d k'}{(2\pi)^d} W_{\boldsymbol{k}'\boldsymbol{k}} (1 - \cos\theta_{\boldsymbol{k}\boldsymbol{k}'}), \tag{1.1}$$

where $W_{\boldsymbol{k}'\boldsymbol{k}}$ is the transition rate from $\boldsymbol{k}$ state to $\boldsymbol{k}'$ state. The inverse relaxation time

is a weighted average of the scattering probability in which the forward scattering $(\theta_{\boldsymbol{kk'}} = 0)$ receives reduced weight.
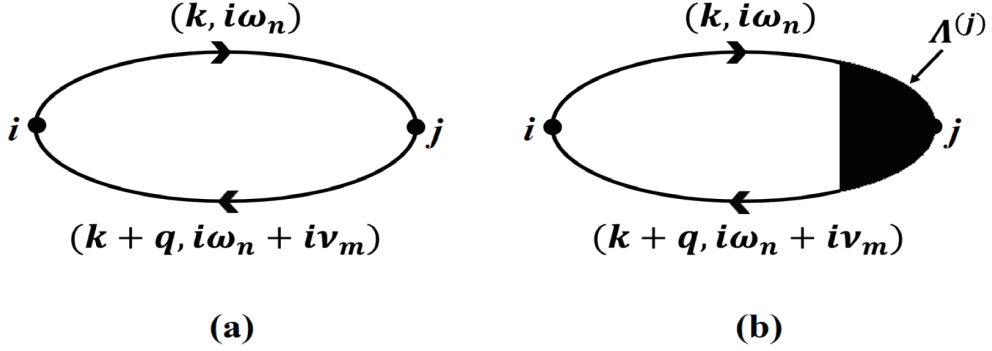


Figure 1.1: Schematic diagrams for (a) Drude conductivity without the $(1 - \cos\theta)$ factor, (b) ladder diagrams giving the $(1 - \cos\theta)$ factor

In a diagrammatic approach, one can study transport by incorporating relevant corrections into the current-current correlation function. In the semiclassical regime, ladder diagrams gives the dominant correction. For an isotropic system, the ladder vertex corrections yield the same result as the Boltzmann transport theory [7, 8], as shown in Fig. 1.1. The single bubble diagram [Fig. 1.1(a)] captures the Drude conductivity with the quasiparticle lifetime $\tau_{\boldsymbol{k}}^{\mathrm{qp}}$, which does not contain the $(1 - \cos\theta)$ factor, whereas ladder diagrams [Fig. 1.1(b)] give the leading-order corrections to the current vertex from impurity scattering, which yield the $(1 - \cos\theta)$ factor replacing $\tau_{\boldsymbol{k}}^{\mathrm{qp}}$ by the transport relaxation time $\tau_{\boldsymbol{k}}^{\mathrm{tr}}$ in Eq. (1.1).

Consideration of further diagrams, called maximally crossed diagrams, enables us to study transport in the quantum regime. These diagrams play a crucial role in the quantum regime in that the crossings of interaction lines induce a reduction factor of order $\mathcal{O}(\frac{1}{k_{\mathrm{F}}\ell_e})$. The maximally crossed diagrams capture an inherent negative correction to dc conductivity, so-called weak localization. Weak localization emerges

as electrons obtain an enhanced probability of backscattering due to a quantum interference effect. In contrast, electrons carrying $\pi$ Berry phase lead to a positive quantum correction to dc conductivity, which is referred to as weak antilocalization. For isotropic systems, one can straightforwardly obtain an analytical expression for these corrections .

In anisotropic systems, transport theory requires more care. As for the semiclassical Boltzmann approach, the relaxation time is not simply given by Eq. (1.1); rather its relation is generalized to coupled integral equations relating the relaxation times at different states [9–14]. Many materials of current interest, such as nodal-line semimetals [15, 16], multi-Weyl semimetals [17], and few-layer black phosphorus [18–20], have an anisotropic Fermi surface. In order to describe transport in these materials, one should properly consider the effects of the lattice anisotropy.

Although the majority of materials have an anisotropic Fermi surface, diagrammatic approach to calculate the dc conductivity of disordered anisotropic systems has been elusive. Motivated by this, we develop a diagrammatic formalism for computing dc conductivity, which can be applied to a general anisotropic system.

The rest of this thesis is organized as follows.

In chapter 2, we review the Boltzmann transport theory in anisotropic multiband systems for both elastic and inelastic scatterings.

In chapter 3, using a diagrammatic approach, we develop a theory for the vertex corrections in anisotropic multiband systems, proving that the diagrammatic approach gives the same result as the Boltzmann approach. We verify the validity of the theory by testing the Ward identity.

In chapter 4, we construct a weak localization theory in anisotropic systems. To this end, we derive a Cooperon ansatz of the Bethe-Salpeter equation, which captures the anisotropy and Berry phase effect of the system.

In chapter 5, we apply the generalized weak localization theory to various phases of few-layer black phosphorus. We predict a nontrivial power-law dependence on the

magnetic field at the semi-Dirac transition point. We demonstrate that the ratio between the magnetoconductivity and the Boltzmann conductivity is independent of the direction, even in strongly anisotropic systems.

In chapter 6, we conclude this thesis by giving a summary.

# Chapter 2

# Semiclassical Boltzmann transport theory

In this chapter, we provide the semiclassical approach to calculate transport properties. We use the semiclassical Boltzmann theory within the first-order Born approximation, which is known to be valid in the weak scattering limit [21–23].

## 2.1 Elastic scattering

In this section, we briefly review the semiclassical Boltzmann theory in $d$-dimensional anisotropic multiband systems for elastic scattering. In the following derivation, we assume that electrons are scattered from randomly-distributed impurities. We set the reduced Planck constant $\hbar$ to 1 for convenience.

We start by considering the phase space of a semiclassical system. Let $f(\boldsymbol{r}, \boldsymbol{k}; t)$ denote the particle distribution function of an electron at the state $\boldsymbol{k}$ at position $\boldsymbol{r}$ at time $t$. The rate of change of $f(\boldsymbol{r}, \boldsymbol{k}; t)$ with respect to time satisfies the following equation:

$$\frac{df}{dt} = \frac{\partial f}{\partial \boldsymbol{r}} \cdot \boldsymbol{v_k} + \frac{\partial f}{\partial \boldsymbol{k}} \cdot \dot{\boldsymbol{k}} + \frac{\partial f}{\partial t}, \tag{2.1}$$

where $\boldsymbol{v_k}$ is the velocity at the state $\boldsymbol{k}$. Assuming a homogeneous system without the explicit time dependence in $f(\boldsymbol{r}, \boldsymbol{k}; t) \equiv f_{\boldsymbol{k}}$, Eq. (2.1) reduces to $\frac{df}{dt} = \frac{\partial f_{\boldsymbol{k}}}{\partial \boldsymbol{k}} \cdot \dot{\boldsymbol{k}}$. When there is no collision in the system, the number of particles in a phase volume element

5

is conserved, and thus $\frac{df}{dt} = 0$. In the presence of collision, the collision integral reads

$$\left(\frac{df}{dt}\right)_{\mathrm{c}} = \int \frac{d^d k'}{(2\pi)^d} \left[ W_{\boldsymbol{k}\boldsymbol{k}'} f_{\boldsymbol{k}'} (1 - f_{\boldsymbol{k}}) - W_{\boldsymbol{k}'\boldsymbol{k}} f_{\boldsymbol{k}} (1 - f_{\boldsymbol{k}'}) \right],$$

(2.2)

where $W_{\boldsymbol{k}'\boldsymbol{k}}$ is the transition rate from $\boldsymbol{k}$ to $\boldsymbol{k}'$. The first term in the right-hand side of Eq. (2.2) describes the probability per unit time that an electron is scattered into a state $\boldsymbol{k}$ and the second term describes the probability per unit time that an electron in a state $\boldsymbol{k}$ is scattered out. The Boltzmann transport equation is given by $\left(\frac{df}{dt}\right) = \left(\frac{df}{dt}\right)_{\mathrm{c}}$. For multiband systems, the Boltzmann transport equation can be generalized as

$$\frac{\partial f_{\alpha,\boldsymbol{k}}}{\partial \boldsymbol{k}} \cdot \dot{\boldsymbol{k}} = \sum_{\alpha'} \int \frac{d^d k'}{(2\pi)^d} \{ W_{\alpha,\boldsymbol{k};\alpha',\boldsymbol{k}'} f_{\alpha',\boldsymbol{k}'} (1 - f_{\alpha,\boldsymbol{k}})$$

$$- W_{\alpha',\boldsymbol{k}';\alpha,\boldsymbol{k}} f_{\alpha,\boldsymbol{k}} (1 - f_{\alpha',\boldsymbol{k}'}) \},$$

(2.3)

where $\alpha$ and $\alpha'$ denote band indices.

For elastic scattering, the transition rate $W_{\alpha',\boldsymbol{k}';\alpha,\boldsymbol{k}}$ is given by

$$W_{\alpha',\boldsymbol{k}';\alpha,\boldsymbol{k}} = 2\pi n_{\mathrm{imp}} |V_{\alpha',\boldsymbol{k}';\alpha,\boldsymbol{k}}|^2 \delta(\xi_{\alpha,\boldsymbol{k}} - \xi_{\alpha',\boldsymbol{k}'}),$$

(2.4)

where $n_{\mathrm{imp}}$ is the impurity density, $V_{\alpha',\boldsymbol{k}';\alpha,\boldsymbol{k}} = \langle \alpha', \boldsymbol{k}' | V | \alpha, \boldsymbol{k} \rangle$ is the matrix element of the impurity potential $V$, which describes a scattering from $(\alpha, \boldsymbol{k})$ to $(\alpha', \boldsymbol{k}')$, and $\xi_{\alpha,\boldsymbol{k}} \equiv \varepsilon_{\alpha,\boldsymbol{k}} - \mu$ is the energy of an electron at the state $(\alpha, \boldsymbol{k})$ measured from the chemical potential $\mu$. Here, the effect of electron-electron interactions can be taken into account through the screening of the impurity potential. Note that $W_{\alpha,\boldsymbol{k};\alpha',\boldsymbol{k}'} = W_{\alpha',\boldsymbol{k}';\alpha,\boldsymbol{k}}$; thus, Eq. (2.3) reduces to

$$\frac{\partial f_{\alpha,\boldsymbol{k}}}{\partial \boldsymbol{k}} \cdot \dot{\boldsymbol{k}} = \sum_{\alpha'} \int \frac{d^d k'}{(2\pi)^d} W_{\alpha',\boldsymbol{k}';\alpha,\boldsymbol{k}} (f_{\alpha',\boldsymbol{k}'} - f_{\alpha,\boldsymbol{k}}).$$

(2.5)

In the presence of a small external electric field, we assume that $f_{\alpha,\boldsymbol{k}}$ deviates slightly from $f_{\alpha,\boldsymbol{k}}^0$:

$$f_{\alpha,\boldsymbol{k}} = f_{\alpha,\boldsymbol{k}}^0 + \delta f_{\alpha,\boldsymbol{k}},$$

(2.6)

where $f^0_{\alpha,\boldsymbol{k}} \equiv f^0(\xi_{\alpha,\boldsymbol{k}}) = \left[e^{\beta\xi_{\alpha,\boldsymbol{k}}} + 1\right]^{-1}$ is the Fermi–Dirac distribution function in equilibrium with $\beta = \frac{1}{k_{\mathrm{B}}T}$. We assume that the deviation $\delta f_{\alpha,\boldsymbol{k}}$ can be parameterized up to first order of the electric field $\boldsymbol{E}$ as follows [12–14]:

$$\delta f_{\alpha,\boldsymbol{k}} = (-e) \sum_i E^{(i)} v^{(i)}_{\alpha,\boldsymbol{k}} \tau^{(i)}_{\alpha,\boldsymbol{k}} S^0(\xi_{\alpha,\boldsymbol{k}}), \tag{2.7}$$

where $S^0(\xi) = -\frac{\partial f^0(\xi)}{\partial \xi} = \beta f^0(\xi)\left[1 - f^0(\xi)\right]$, and $v^{(i)}_{\alpha,\boldsymbol{k}}$ and $\tau^{(i)}_{\alpha,\boldsymbol{k}}$ are the velocity and transport relaxation time along the $i$th direction at the state $(\alpha, \boldsymbol{k})$, respectively. Inserting Eq. (2.7) into Eq. (2.5), we have an integral equation relating the relaxation times at different states

$$1 = \sum_{\alpha'} \int \frac{d^d k'}{(2\pi)^d} W_{\alpha',\boldsymbol{k}';\alpha,\boldsymbol{k}} \left( \tau^{(i)}_{\alpha,\boldsymbol{k}} - \frac{v^{(i)}_{\alpha',\boldsymbol{k}'}}{v^{(i)}_{\alpha,\boldsymbol{k}}} \tau^{(i)}_{\alpha',\boldsymbol{k}'} \right), \tag{2.8}$$

which reduces to Eq. (1.1) in an isotropic single-band system.

The deviation of the electron distribution function from the equilibrium value gives rise to the current density

$$J^{(i)} = g \sum_{\alpha} \int \frac{d^d k}{(2\pi)^d} (-e) v^{(i)}_{\alpha,\boldsymbol{k}} \delta f_{\alpha,\boldsymbol{k}} = \sum_j \sigma_{ij} E^{(j)}, \tag{2.9}$$

where $g$ is the degeneracy factor and $\sigma_{ij}$ is a matrix element of the conductivity tensor given by

$$\sigma_{ij} = g e^2 \sum_{\alpha} \int \frac{d^d k}{(2\pi)^d} S^0(\xi_{\alpha,\boldsymbol{k}}) v^{(i)}_{\alpha,\boldsymbol{k}} v^{(j)}_{\alpha,\boldsymbol{k}} \tau^{(j)}_{\alpha,\boldsymbol{k}}. \tag{2.10}$$

## 2.2 Inelastic scattering

For inelastic scattering, such as phonon-mediated scattering, Eq. (2.8) is no longer valid and the principle of detailed balance should be considered [24]:

$$W_{\alpha',\boldsymbol{k}';\alpha,\boldsymbol{k}} f^0_{\alpha,\boldsymbol{k}}(1 - f^0_{\alpha',\boldsymbol{k}'}) = W_{\alpha,\boldsymbol{k};\alpha',\boldsymbol{k}'} f^0_{\alpha',\boldsymbol{k}'}(1 - f^0_{\alpha,\boldsymbol{k}}). \tag{2.11}$$

Expanding up to first order of $\delta f$, Eq. (2.3) reduces to

$$
\frac{\partial f^0_{\alpha,\boldsymbol{k}}}{\partial \boldsymbol{k}} \cdot \dot{\boldsymbol{k}} = \sum_{\alpha'} \int \frac{d^d k'}{(2\pi)^d} W_{\alpha',\boldsymbol{k}';\alpha,\boldsymbol{k}}
$$
$$
\times \left( \frac{f^0_{\alpha,\boldsymbol{k}}}{f^0_{\alpha',\boldsymbol{k}'}} \delta f_{\alpha',\boldsymbol{k}'} - \frac{1 - f^0_{\alpha',\boldsymbol{k}'}}{1 - f^0_{\alpha,\boldsymbol{k}}} \delta f_{\alpha,\boldsymbol{k}} \right). \tag{2.12}
$$

Using the parameterization in Eq. (2.7), we obtain an integral equation for inelastic scattering:

$$
1 = \sum_{\alpha'} \int \frac{d^d k'}{(2\pi)^d} W_{\alpha',\boldsymbol{k}';\alpha,\boldsymbol{k}}
$$
$$
\times \left( \tau^{(i)}_{\alpha,\boldsymbol{k}} - \frac{v^{(i)}_{\alpha',\boldsymbol{k}'}}{v^{(i)}_{\alpha,\boldsymbol{k}}} \tau^{(i)}_{\alpha',\boldsymbol{k}'} \right) \left( \frac{1 - f^0_{\alpha',\boldsymbol{k}'}}{1 - f^0_{\alpha,\boldsymbol{k}}} \right). \tag{2.13}
$$

Note that the integral equation for inelastic scattering is different from that for elastic scattering by the factor $\left( \frac{1 - f^0_{\alpha',\boldsymbol{k}'}}{1 - f^0_{\alpha,\boldsymbol{k}}} \right)$.

For phonon scattering, the transition rate $W_{\alpha',\boldsymbol{k}';\alpha,\boldsymbol{k}}$ is given by [25]

$$
W_{\alpha',\boldsymbol{k}';\alpha,\boldsymbol{k}} = 2\pi \sum_{\lambda} |\langle \alpha', \boldsymbol{k}' | M_\lambda | \alpha, \boldsymbol{k} \rangle|^2
$$
$$
\times \{ [n_{\mathrm{B}}(\Omega_{\lambda,\boldsymbol{q}}) + 1]\, \delta(\xi_{\alpha',\boldsymbol{k}'} - \xi_{\alpha,\boldsymbol{k}} + \Omega_{\lambda,\boldsymbol{q}})
$$
$$
+ n_{\mathrm{B}}(\Omega_{\lambda,\boldsymbol{q}})\delta(\xi_{\alpha',\boldsymbol{k}'} - \xi_{\alpha,\boldsymbol{k}} - \Omega_{\lambda,\boldsymbol{q}}) \}, \tag{2.14}
$$

where $n_{\mathrm{B}}(\Omega_{\lambda,\boldsymbol{q}}) = \left[ e^{\beta \Omega_{\lambda,q}} - 1 \right]^{-1}$ is the Bose–Einstein distribution function, and $M_\lambda$ denotes the electron-phonon interaction for the phonon polarization $\lambda$. Here, the first (second) term on the right-hand side of Eq. (2.14) denotes the emission (absorption) of a phonon with momentum $\boldsymbol{q} = \pm(\boldsymbol{k} - \boldsymbol{k}')$ and frequency $\Omega_{\lambda,\boldsymbol{q}}$. In this thesis, umklapp processes are neglected since we are interested in the weak scattering limit where normal processes are dominant [26].

# Chapter 3

# Ladder vertex corrections

In this chapter, we develop a theory for the vertex corrections to the dc conductivity for elastic and inelastic scatterings in $d$-dimensional anisotropic multiband systems, and verify that the results are consistent with those obtained from the Boltzmann approach in chapter 2.

The dc conductivity can be obtained by taking the long wavelength limit and then the static limit as follows [7]:

$$\sigma_{ij}^{\mathrm{dc}} = -\lim_{\nu \to 0} \frac{1}{\nu} \mathrm{Im} \Pi_{ij}(\boldsymbol{q} = 0, \nu), \tag{3.1}$$

where $\Pi_{ij}(\boldsymbol{q}, \nu)$ is the retarded current-current response function, which is obtained using the analytic continuation $i\nu_m \to \nu + i0^+$ of the current-current response function $\Pi_{ij}(\boldsymbol{q}, i\nu_m)$. First, we consider the single bubble diagram without the vertex corrections [Fig. 1.1(a)]

$$\Pi_{ij}(i\nu_m) = \frac{ge^2}{\beta\mathcal{V}} \sum_{\alpha,\alpha',\boldsymbol{k},i\omega_n} \mathcal{G}_\alpha(\boldsymbol{k}, i\omega_n) v_{\alpha,\alpha'}^{(i)}(\boldsymbol{k}, \boldsymbol{k}) \mathcal{G}_{\alpha'}(\boldsymbol{k}, i\omega_n + i\nu_m) v_{\alpha',\alpha}^{(j)}(\boldsymbol{k}), \tag{3.2}$$

where $\Pi_{ij}(i\nu_m) = \Pi_{ij}(\boldsymbol{q} = 0, i\nu_m)$, $\omega_n$ and $\nu_m$ are fermionic and bosonic Matsubara frequencies, respectively, $\mathcal{V}$ is the volume of the system, $\mathcal{G}_\alpha(\boldsymbol{k}, i\omega_n)$ is the interacting Green's function, and $v_{\alpha',\alpha}^{(j)}(\boldsymbol{k}) = \langle \alpha', \boldsymbol{k} | \hat{v}^{(j)} | \alpha, \boldsymbol{k} \rangle$ is the matrix element of the velocity operator $\hat{v}^{(j)} = \frac{\partial \hat{H}}{\partial k_j}$ along the $j$th direction. The velocity matrix element can be

expressed as

$$v_{\alpha',\alpha}^{(j)}(\boldsymbol{k}) = v_{\alpha,\boldsymbol{k}}^{(j)} \langle \alpha', \boldsymbol{k} | \alpha, \boldsymbol{k} \rangle + (\varepsilon_{\alpha,\boldsymbol{k}} - \varepsilon_{\alpha',\boldsymbol{k}}) \langle \alpha', \boldsymbol{k} | \frac{\partial}{\partial k_j} | \alpha, \boldsymbol{k} \rangle. \qquad (3.3)$$

In the $\nu \to 0$ limit, the second term in Eq. (3.3) does not contribute to $\Pi_{ij}(i\nu_m)$ as finite energy transfer between $(\alpha', \boldsymbol{k})$ and $(\alpha, \boldsymbol{k})$ is not allowed in the single bubble diagram. By choosing an orthonormal basis set, the right-hand side of Eq. (3.3) simply reduces to $v_{\alpha,\boldsymbol{k}}^{(j)} \delta_{\alpha',\alpha}$, and only diagonal elements of the velocity matrix remain in Eq. (3.2).

Incorporating the ladder diagrams, we finally obtain the current-current response function supplemented with the vertex corrections as follows [Fig. 1.1(b)]:

$$\Pi_{ij}(i\nu_m) = \frac{ge^2}{\beta \mathcal{V}} \sum_{\alpha,\boldsymbol{k},i\omega_n} \mathcal{G}_\alpha(\boldsymbol{k}, i\omega_n) v_{\alpha,\boldsymbol{k}}^{(i)} \mathcal{G}_\alpha(\boldsymbol{k}, i\omega_n + i\nu_m)$$

$$\times v_{\alpha,\boldsymbol{k}}^{(j)} \Lambda_\alpha^{(j)}(\boldsymbol{k}, i\omega_n, i\omega_n + i\nu_m), \qquad (3.4)$$

where $v_{\alpha,\boldsymbol{k}}^{(j)} \Lambda_\alpha^{(j)}(\boldsymbol{k}, i\omega_n, i\omega_n + i\nu_m)$ is the vertex corresponding to the current density operator along the $j$th direction. Note that we only included the diagonal elements of the velocity matrix, as discussed above.

To compute the dc conductivity using a diagrammatic method, we can either perform the Matsubara frequency summation first or the momentum integral first. In the following, we use the former method where the frequency summation is performed first, and present the other method in chapter 3.4.

## 3.1   Impurity scattering

As for elastic scattering, we consider randomly distributed impurities. We consider the effect of impurities using the disorder-averaged Green's function

$$\mathcal{G}_\alpha(\boldsymbol{k}, i\omega_n) = \frac{1}{i\omega_n - \xi_{\alpha,\boldsymbol{k}} - \Sigma_\alpha(\boldsymbol{k}, i\omega_n)}, \qquad (3.5)$$

where $\Sigma_\alpha(\boldsymbol{k}, i\omega_n)$ is the electron self-energy from impurity scattering. The imaginary part of the self-energy can be related to the quasiparticle lifetime $\tau_{\alpha,\boldsymbol{k}}^{\mathrm{qp}}$ as $\mathrm{Im}\Sigma_\alpha(\boldsymbol{k}, i\omega_n) =$

$-\frac{1}{2\tau_{\alpha,k}^{\text{qp}}}\text{sgn}(\omega_n)$. Assuming small impurity density, we obtain the inverse of the quasi-particle lifetime

$$\frac{1}{\tau_{\alpha,k}^{\text{qp}}} = 2\pi n_{\text{imp}} \sum_{\alpha'} \int \frac{d^d k'}{(2\pi)^d} |V_{\alpha',k';\alpha,k}|^2 \delta(\xi_{\alpha,k} - \xi_{\alpha',k'})$$
$$= \sum_{\alpha'} \int \frac{d^d k'}{(2\pi)^d} W_{\alpha',k';\alpha,k}. \tag{3.6}$$

Within the ladder approximation, the vertex correction is approximated by a sum of ladder diagrams given by a self-consistent form as follows [Fig. 3.1]:

$$v_{\alpha,k}^{(j)} \Lambda_{\alpha}^{(j)}(k, i\omega_n, i\omega_n + i\nu_m) = v_{\alpha,k}^{(j)} + \frac{n_{\text{imp}}}{\mathcal{V}} \sum_{\alpha',k'} |V_{\alpha',k';\alpha,k}|^2 \mathcal{G}_{\alpha'}(k', i\omega_n) \tag{3.7}$$
$$\times v_{\alpha',k'}^{(j)} \Lambda_{\alpha'}^{(j)}(k', i\omega_n, i\omega_n + i\nu_m) \mathcal{G}_{\alpha'}(k', i\omega_n + i\nu_m).$$

As the form of the self-consistent equation in Eq. (3.7) is analogous to Eq. (2.8), $\Lambda^{(j)}$ can be related to the transport relaxation time. Here, we derive this relation rigorously.
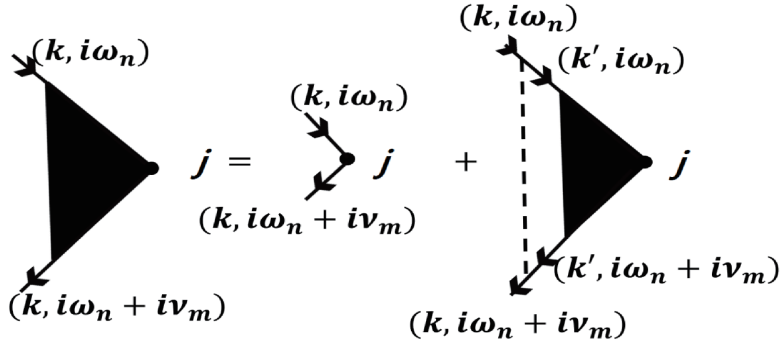


Figure 3.1: Diagrams for the ladder vertex corrections for elastic scattering

Let us first compute the current-current correlation function in Eq. (3.4):

$$\Pi_{ij}(i\nu_m) \equiv \frac{1}{\beta} \sum_{i\omega_n} P(i\omega_n, i\omega_n + i\nu_m)$$
$$= -\oint_C \frac{dz}{2\pi i} \frac{P(z, z + i\nu_m)}{e^{\beta z} + 1}, \tag{3.8}$$

11

where we introduce a complex function $P(i\omega_n, i\omega_n + i\nu_m)$, whose summation can be performed via integration along the contour $C$ shown in Fig. 3.2. Note that the contour integral in Eq. (3.8) has poles at $z = i\omega_n$.
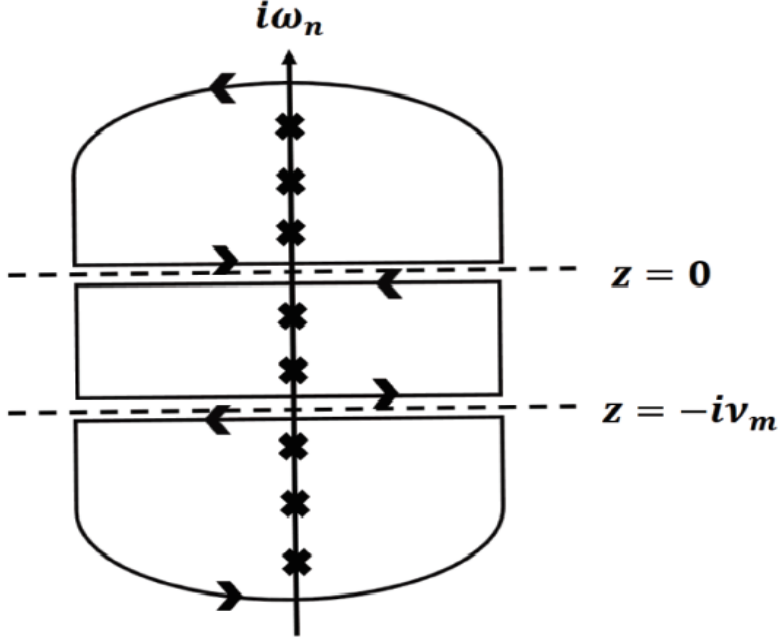


Figure 3.2: Contour integral along $C$, which has two branch cuts along the axes $z = 0$ and $z = -i\nu_m$

Following chapter 8 of Mahan [7], we compute the contour integral in Eq. (3.8):

$$\Pi_{ij}(i\nu_m) = -\oint_C \frac{dz}{2\pi i} f^0(z) P(z, z + i\nu_m) \tag{3.9}$$
$$= \int \frac{d\xi}{2\pi i} f^0(\xi) \left[ -P(\xi + i0^+, \xi + i\nu_m) + P(\xi - i0^+, \xi + i\nu_m) \right.$$
$$\left. - P(\xi - i\nu_m, \xi + i0^+) + P(\xi - i\nu_m, \xi - i0^+) \right].$$

After performing the analytic continuation $(i\nu_m \to \nu + i0^+)$, we have

$$\Pi_{ij}^{\text{R}}(\nu) = \int \frac{d\xi}{2\pi i} \{ [f^0(\xi) - f^0(\xi + \nu)] P^{\text{AR}}(\xi, \xi + \nu) \tag{3.10}$$
$$- f^0(\xi) P^{\text{RR}}(\xi, \xi + \nu) + f^0(\xi + \nu) P^{\text{AA}}(\xi, \xi + \nu) \},$$

12

where the superscripts A and R represent advanced and retarded functions, respectively. Thus, in the $\nu \to 0$ limit, the dc conductivity can be rewritten as

$$\sigma_{ij} = \frac{ge^2}{2\pi} \int d\xi S^0(\xi)[P^{\mathrm{AR}}(\xi,\xi) - \mathrm{Re}P^{\mathrm{RR}}(\xi,\xi)], \qquad (3.11)$$

which includes the $P^{\mathrm{AR}}(\xi,\xi)$ and $P^{\mathrm{RR}}(\xi,\xi)$ terms in the integrand.

Here, we show that only the $P^{\mathrm{AR}}(\xi,\xi)$ term contributes to the dc conductivity in the limit of small impurity density. Before computing each term, we note several useful formulas pertaining to the spectral function $A_\alpha(\boldsymbol{k},\xi) = -2\mathrm{Im}G_\alpha^{\mathrm{R}}(\boldsymbol{k},\xi)$:

$$\lim_{\Delta_{\alpha,\boldsymbol{k}} \to 0} A_\alpha(\boldsymbol{k},\xi) = 2\pi\delta(\xi - \xi_{\alpha,\boldsymbol{k}}), \qquad (3.12a)$$

$$\lim_{\Delta_{\alpha,\boldsymbol{k}} \to 0} A_\alpha^2(\boldsymbol{k},\xi) = \frac{2\pi\delta(\xi - \xi_{\alpha,\boldsymbol{k}})}{\Delta_{\alpha,\boldsymbol{k}}}, \qquad (3.12b)$$

where $\Delta_{\alpha,\boldsymbol{k}} \equiv \frac{1}{2\tau_{\alpha,\boldsymbol{k}}^{\mathrm{qp}}}$. Note that, in the $\Delta_{\alpha,\boldsymbol{k}} \to 0$ limit, or equivalently in the $n_{\mathrm{imp}} \to 0$ limit, the spectral function reduces to a delta function.

First, let us evaluate the contribution of the $P^{\mathrm{RR}}(\xi,\xi)$ term:

$$P^{\mathrm{RR}}(\xi,\xi) = \frac{ge^2}{\mathcal{V}} \sum_{\alpha,\boldsymbol{k}} v_{\alpha,\boldsymbol{k}}^{(i)} G_\alpha^{\mathrm{R}}(\boldsymbol{k},\xi) v_{\alpha,\boldsymbol{k}}^{(j)} \Lambda_\alpha^{(j)\mathrm{RR}}(\boldsymbol{k},\xi,\xi) G_\alpha^{\mathrm{R}}(\boldsymbol{k},\xi). \qquad (3.13)$$

In the $n_{\mathrm{imp}} \to 0$ limit, the product of the two Green's functions vanishes and the contribution of $P^{\mathrm{RR}}(\xi,\xi)$ to the dc conductivity becomes negligible [7].

Subsequently, let us compute the $P^{\mathrm{AR}}(\xi,\xi)$ term as follows:

$$P^{\mathrm{AR}}(\xi,\xi) = \frac{ge^2}{\mathcal{V}} \sum_{\alpha,\boldsymbol{k}} v_{\alpha,\boldsymbol{k}}^{(i)} G_\alpha^{\mathrm{A}}(\boldsymbol{k},\xi) v_{\alpha,\boldsymbol{k}}^{(j)} \Lambda_\alpha^{(j)\mathrm{AR}}(\boldsymbol{k},\xi,\xi) G_\alpha^{\mathrm{R}}(\boldsymbol{k},\xi)$$

$$= \frac{2\pi ge^2}{\mathcal{V}} \sum_{\alpha,\boldsymbol{k}} v_{\alpha,\boldsymbol{k}}^{(i)} v_{\alpha,\boldsymbol{k}}^{(j)} \tau_{\alpha,\boldsymbol{k}}^{\mathrm{qp}} \delta(\xi - \xi_{\alpha,\boldsymbol{k}}) \Lambda_\alpha^{(j)\mathrm{AR}}(\boldsymbol{k},\xi,\xi). \qquad (3.14)$$

Therefore, the dc conductivity can be simplified as

$$\sigma_{ij} = \frac{1}{2\pi} \int d\xi S^0(\xi) P^{\mathrm{AR}}(\xi,\xi)$$

$$= \frac{ge^2}{\mathcal{V}} \sum_{\alpha,\boldsymbol{k}} S^0(\xi_{\alpha,\boldsymbol{k}}) v_{\alpha,\boldsymbol{k}}^{(i)} v_{\alpha,\boldsymbol{k}}^{(j)} \tau_{\alpha,\boldsymbol{k}}^{\mathrm{qp}} \Lambda_\alpha^{(j)\mathrm{AR}}(\boldsymbol{k},\xi_{\alpha,\boldsymbol{k}},\xi_{\alpha,\boldsymbol{k}}). \qquad (3.15)$$

13

Comparing Eq. (3.15) with Eq. (2.10), it is natural to relate $\Lambda^{(j)}$ to the transport relaxation time along the $j$th direction. After analytic continuation, Eq. (3.7) reduces to

$$\Lambda_\alpha^{(j)\mathrm{AR}}(\boldsymbol{k},\xi,\xi) = 1 + \sum_{\alpha'} \int \frac{d^d k'}{(2\pi)^d} W_{\alpha',\boldsymbol{k}';\alpha,\boldsymbol{k}} \frac{v_{\alpha',\boldsymbol{k}'}^{(j)}}{v_{\alpha,\boldsymbol{k}}^{(j)}} \tau_{\alpha',\boldsymbol{k}'}^{\mathrm{qp}} \Lambda_{\alpha'}^{(j)\mathrm{AR}}(\boldsymbol{k}',\xi,\xi). \quad (3.16)$$

Defining the transport relaxation time along the $j$th direction as

$$\tau_{\alpha,\boldsymbol{k}}^{(j)} \equiv \tau_{\alpha,\boldsymbol{k}}^{\mathrm{qp}} \Lambda_\alpha^{(j)\mathrm{AR}}(\boldsymbol{k},\xi_{\alpha,\boldsymbol{k}},\xi_{\alpha,\boldsymbol{k}}). \quad (3.17)$$

we can rewrite Eq. (3.16) as

$$\frac{\tau_{\alpha,\boldsymbol{k}}^{(j)}}{\tau_{\alpha,\boldsymbol{k}}^{\mathrm{qp}}} = 1 + \sum_{\alpha'} \int \frac{d^d k'}{(2\pi)^d} W_{\alpha',\boldsymbol{k}';\alpha,\boldsymbol{k}} \frac{v_{\alpha',\boldsymbol{k}'}^{(j)}}{v_{\alpha,\boldsymbol{k}}^{(j)}} \tau_{\alpha',\boldsymbol{k}'}^{(j)}. \quad (3.18)$$

Using the definition of the quasiparticle lifetime in Eq. (3.6), we obtain an integral equation for the transport relaxation time for elastic scattering in anisotropic multiband systems as

$$1 = \sum_{\alpha'} \int \frac{d^d k'}{(2\pi)^d} W_{\alpha',\boldsymbol{k}';\alpha,\boldsymbol{k}} \left( \tau_{\alpha,\boldsymbol{k}}^{(j)} - \frac{v_{\alpha',\boldsymbol{k}'}^{(j)}}{v_{\alpha,\boldsymbol{k}}^{(j)}} \tau_{\alpha',\boldsymbol{k}'}^{(j)} \right), \quad (3.19)$$

which is the same as the semiclassical result in Eq. (2.8). Furthermore, using the definition of the transport relaxation time, we can easily verify that Eq. (3.15) is consistent with Eq. (2.10) obtained from the semiclassical approach.

## 3.2 Phonon scattering

As in the case of elastic scattering, we develop a theory for the vertex corrections for inelastic scattering. Here, we specifically consider phonon-mediated scattering, which yields intrinsic resistivity in a metal.

The self-consistent equation of the vertex part for phonon scattering is given by

[Fig. 3.3]

$$v_{\alpha,\boldsymbol{k}}^{(j)}\Lambda_\alpha^{(j)}(\boldsymbol{k}, i\omega_n, i\omega_n + i\nu_m) = v_{\alpha,\boldsymbol{k}}^{(j)} - \frac{1}{\beta\mathcal{V}}\sum_{\alpha',\boldsymbol{q},iq_l,\lambda} |\langle\alpha',\boldsymbol{k}+\boldsymbol{q}|M_\lambda|\alpha,\boldsymbol{k}\rangle|^2 D_\lambda(\boldsymbol{q}, iq_l)$$

$$\times \mathcal{G}_{\alpha'}(\boldsymbol{k}+\boldsymbol{q}, i\omega_n + iq_l)\mathcal{G}_{\alpha'}(\boldsymbol{k}+\boldsymbol{q}, i\omega_n + iq_l + i\nu_m)$$

$$\times v_{\alpha',\boldsymbol{k}+\boldsymbol{q}}^{(j)}\Lambda_{\alpha'}^{(j)}(\boldsymbol{k}+\boldsymbol{q}, i\omega_n + iq_l, i\omega_n + iq_l + i\nu_m),$$

(3.20)

where $q_l$ is a bosonic Matsubara frequency and $D_\lambda(\boldsymbol{q}, iq_l) = \frac{2\Omega_{\lambda,\boldsymbol{q}}}{(iq_l)^2 - \Omega_{\lambda,\boldsymbol{q}}^2}$ is the non-interacting phonon Green's function with the renormalized phonon frequency $\Omega_{\lambda,\boldsymbol{q}}$. Eq. (3.20) can be rewritten as

$$\Lambda_\alpha^{(j)}(\boldsymbol{k}, i\omega_n, i\omega_n + i\nu_m) = 1 - \sum_{\alpha',\lambda}\int \frac{d^d q}{(2\pi)^d}|\langle\alpha',\boldsymbol{k}+\boldsymbol{q}|M_\lambda|\alpha,\boldsymbol{k}\rangle|^2\frac{v_{\alpha',\boldsymbol{k}+\boldsymbol{q}}^{(j)}}{v_{\alpha,\boldsymbol{k}}^{(j)}}$$

$$\times \frac{1}{\beta}\sum_{iq_l} Q(iq_l + i\omega_n, iq_l + i\omega_n + i\nu_m), \quad (3.21)$$

where

$$Q(iq_l + i\omega_n, iq_l + i\omega_n + i\nu_m) \equiv \mathcal{G}_{\alpha'}(\boldsymbol{k}+\boldsymbol{q}, iq_l + i\omega_n)\mathcal{G}_{\alpha'}(\boldsymbol{k}+\boldsymbol{q}, iq_l + i\omega_n + i\nu_m)$$

$$\times D_\lambda(\boldsymbol{q}, iq_l)\Lambda_{\alpha'}^{(j)}(\boldsymbol{k}+\boldsymbol{q}, iq_l + i\omega_n, iq_l + i\omega_n + i\nu_m).$$

The summation of $Q(iq_l + i\omega_n, iq_l + i\omega_n + i\nu_m)$ over the bosonic Matsubara frequency $q_l$ can be performed with the aid of a contour integral along the contour $C'$ shown in Fig. 3.4:

$$\oint_{C'} \frac{dz}{2\pi i}\frac{Q(z + i\omega_n, z + i\omega_n + i\nu_m)}{e^{\beta z} - 1}. \quad (3.22)$$

Note that the contour integral in Eq. (3.22) has poles at $z = iq_l$ as well as $z = \pm\Omega_{\lambda,\boldsymbol{q}}$. Therefore, the summation $\mathcal{S}(i\omega_n, i\omega_n + i\nu_m) \equiv \frac{1}{\beta}\sum_{iq_l} Q(iq_l + i\omega_n, iq_l + i\omega_n + i\nu_m)$

15
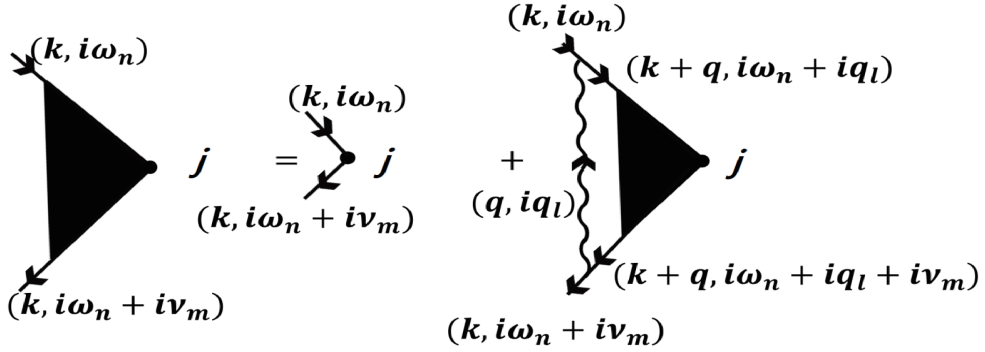
Figure 3.3: Dyson's equation for the ladder vertex corrections for inelastic scattering

can be rewritten as follows:

$$
\begin{aligned}
\mathcal{S}(i\omega_n, i\omega_n + i\nu_m) &= \oint_{C'} \frac{dz}{2\pi i} n_{\mathrm{B}}(z) Q(z + i\omega_n, z + i\omega_n + i\nu_m) \\
&\quad - n_{\mathrm{B}}(\Omega_{\lambda,\boldsymbol{q}}) \mathcal{G}_{\alpha'}(\boldsymbol{k} + \boldsymbol{q}, i\omega_n + \Omega_{\lambda,\boldsymbol{q}} + i\nu_m) \mathcal{G}_{\alpha'}(\boldsymbol{k} + \boldsymbol{q}, i\omega_n + \Omega_{\lambda,\boldsymbol{q}}) \\
&\quad \times \Lambda^{(j)}_{\alpha'}(\boldsymbol{k} + \boldsymbol{q}, i\omega_n + \Omega_{\lambda,\boldsymbol{q}}, i\omega_n + \Omega_{\lambda,\boldsymbol{q}} + i\nu_m) \\
&\quad - [n_{\mathrm{B}}(\Omega_{\lambda,\boldsymbol{q}}) + 1] \mathcal{G}_{\alpha'}(\boldsymbol{k} + \boldsymbol{q}, i\omega_n - \Omega_{\lambda,\boldsymbol{q}} + i\nu_m) \mathcal{G}_{\alpha'}(\boldsymbol{k} + \boldsymbol{q}, i\omega_n - \Omega_{\lambda,\boldsymbol{q}}) \\
&\quad \times \Lambda^{(j)}_{\alpha'}(\boldsymbol{k} + \boldsymbol{q}, i\omega_n - \Omega_{\lambda,\boldsymbol{q}}, i\omega_n - \Omega_{\lambda,\boldsymbol{q}} + i\nu_m), \quad\quad (3.23)
\end{aligned}
$$

where the contour integral can be decomposed as

$$
\oint_{C'} \frac{dz}{2\pi i} n_B(z) Q(z + i\omega_n, z + i\omega_n + i\nu_m)
$$

$$
= -\int \frac{d\xi'}{2\pi i} f^0(\xi') \frac{2\Omega_{\lambda,q}}{(\xi' - i\omega_n)^2 - \Omega_{\lambda,q}^2} \{ \mathcal{G}_{\alpha'}(\boldsymbol{k} + \boldsymbol{q}, \xi' + i0^+) \mathcal{G}_{\alpha'}(\boldsymbol{k} + \boldsymbol{q}, \xi' + i\nu_m)
$$

$$
\times \Lambda_{\alpha'}^{(j)}(\boldsymbol{k} + \boldsymbol{q}, \xi' + i0^+, \xi' + i\nu_m)
$$

$$
- \mathcal{G}_{\alpha'}(\boldsymbol{k} + \boldsymbol{q}, \xi' - i0^+) \mathcal{G}_{\alpha'}(\boldsymbol{k} + \boldsymbol{q}, \xi' + i\nu_m) \Lambda_{\alpha'}^{(j)}(\boldsymbol{k} + \boldsymbol{q}, \xi' - i0^+, \xi' + i\nu_m) \}
$$

$$
- \int \frac{d\xi'}{2\pi i} f^0(\xi') \frac{2\Omega_{\lambda,q}}{(\xi' - i\omega_n - i\nu_m)^2 - \Omega_{\lambda,q}^2} \{ \mathcal{G}_{\alpha'}(\boldsymbol{k} + \boldsymbol{q}, \xi' - i\nu_m) \mathcal{G}_{\alpha'}(\boldsymbol{k} + \boldsymbol{q}, \xi' + i0^+)
$$

$$
\times \Lambda_{\alpha'}^{(j)}(\boldsymbol{k} + \boldsymbol{q}, \xi' - i\nu_m, \xi' + i0^+)
$$

$$
- \mathcal{G}_{\alpha'}(\boldsymbol{k} + \boldsymbol{q}, \xi' - i\nu_m) \mathcal{G}_{\alpha'}(\boldsymbol{k} + \boldsymbol{q}, \xi' - i0^+) \Lambda_{\alpha'}^{(j)}(\boldsymbol{k} + \boldsymbol{q}, \xi' - i\nu_m, \xi' - i0^+) \}.
$$

$$(3.24)$$

To compute $\Lambda^{(j)AR}(\boldsymbol{k}, \xi, \xi)$, let us perform the analytic continuation $i\omega_n \to \xi - i0^+$ and $i\omega_n + i\nu_m \to \xi + \nu + i0^+$. Thus, Eq. (3.23) at $\nu = 0$ reduces to

$$
\mathcal{S}^{AR}(\xi, \xi) = -n_B(\Omega_{\lambda,q}) |G_{\alpha'}^R(\boldsymbol{k} + \boldsymbol{q}, \xi + \Omega_{\lambda,q})|^2 \Lambda_{\alpha'}^{(j)AR}(\boldsymbol{k} + \boldsymbol{q}, \xi + \Omega_{\lambda,q}, \xi + \Omega_{\lambda,q})
$$

$$
- [1 + n_B(\Omega_{\lambda,q})] |G_{\alpha'}^R(\boldsymbol{k} + \boldsymbol{q}, \xi - \Omega_{\lambda,q})|^2 \Lambda_{\alpha'}^{(j)AR}(\boldsymbol{k} + \boldsymbol{q}, \xi - \Omega_{\lambda,q}, \xi - \Omega_{\lambda,q})
$$

$$
- \int \frac{d\xi'}{2\pi i} f^0(\xi') |G_{\alpha'}^R(\boldsymbol{k} + \boldsymbol{q}, \xi')|^2 \Lambda_{\alpha'}^{(j)AR}(\boldsymbol{k} + \boldsymbol{q}, \xi', \xi')
$$

$$
\times \left[ \frac{2\Omega_{\lambda,q}}{(\xi' - \xi - i0^+)^2 - \Omega_{\lambda,q}^2} - \frac{2\Omega_{\lambda,q}}{(\xi' - \xi + i0^+)^2 - \Omega_{\lambda,q}^2} \right]. \qquad (3.25)
$$

The last integration over $\xi'$ can be performed with the aid of the Cauchy principal value

$$
\frac{2\Omega_{\lambda,q}}{(\xi' - \xi - i0^+)^2 - \Omega_{\lambda,q}^2} - \frac{2\Omega_{\lambda,q}}{(\xi' - \xi + i0^+)^2 - \Omega_{\lambda,q}^2} \qquad (3.26)
$$

$$
= 2\pi i \left[ \delta(\xi' - \xi - \Omega_{\lambda,q}) - \delta(\xi' - \xi + \Omega_{\lambda,q}) \right].
$$

Therefore, in the weak-scattering limit, the self-consistent Dyson's equation for inelas-

tic scattering [Eq. (3.20)] can be rewritten as

$$\Lambda_\alpha^{(j)\text{AR}}(\boldsymbol{k},\xi,\xi) = 1 - \sum_{\alpha',\lambda} \int \frac{d^d q}{(2\pi)^d} |\langle \alpha', \boldsymbol{k}+\boldsymbol{q}|M_\lambda|\alpha, \boldsymbol{k}\rangle|^2 \frac{v_{\alpha',\boldsymbol{k}+\boldsymbol{q}}^{(j)}}{v_{\alpha,\boldsymbol{k}}^{(j)}} \mathcal{S}^{\text{AR}}(\xi,\xi)$$

$$= 1 + 2\pi \sum_{\alpha',\lambda} \int \frac{d^d q}{(2\pi)^d} |\langle \alpha', \boldsymbol{k}+\boldsymbol{q}|M_\lambda|\alpha, \boldsymbol{k}\rangle|^2 \frac{v_{\alpha',\boldsymbol{k}+\boldsymbol{q}}^{(j)}}{v_{\alpha,\boldsymbol{k}}^{(j)}} \tau_{\alpha',\boldsymbol{k}+\boldsymbol{q}}^{\text{qp}}$$

$$\times \Lambda_{\alpha'}^{(j)\text{AR}}(\boldsymbol{k}+\boldsymbol{q}, \xi_{\alpha',\boldsymbol{k}+\boldsymbol{q}}, \xi_{\alpha',\boldsymbol{k}+\boldsymbol{q}})$$

$$\times \left\{ \left[ n_{\text{B}}(\Omega_{\lambda,\boldsymbol{q}}) + f^0(\xi + \Omega_{\lambda,\boldsymbol{q}}) \right] \delta(\xi + \Omega_{\lambda,\boldsymbol{q}} - \xi_{\alpha',\boldsymbol{k}+\boldsymbol{q}}) \right.$$

$$\left. + \left[ n_{\text{B}}(\Omega_{\lambda,\boldsymbol{q}}) + 1 - f^0(\xi - \Omega_{\lambda,\boldsymbol{q}}) \right] \delta(\xi - \Omega_{\lambda,\boldsymbol{q}} - \xi_{\alpha',\boldsymbol{k}+\boldsymbol{q}}) \right\}. \quad (3.27)$$
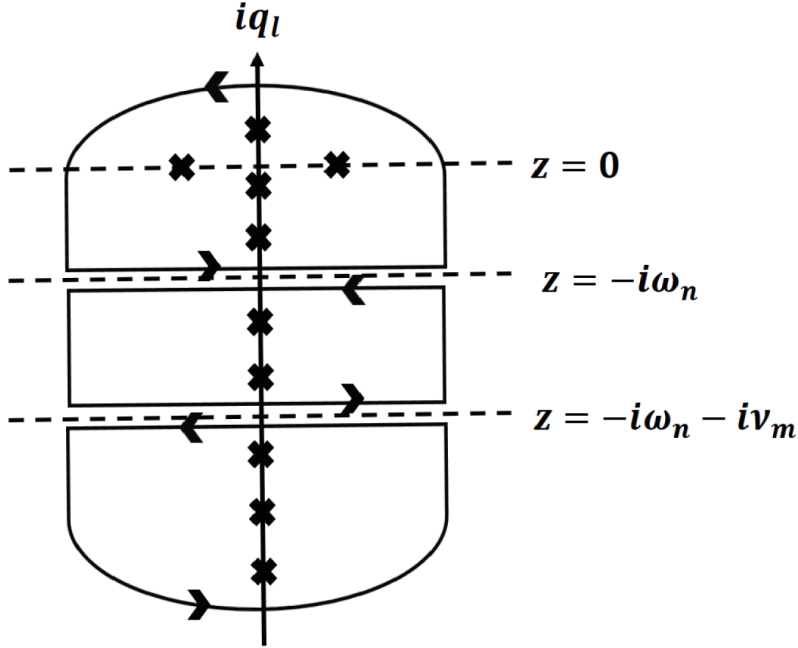


Figure 3.4: Contour integral along $C'$, which has two branch cuts along the axes $z = -i\omega_n$ and $z = -i\omega_n - i\nu_m$

Finally, let us replace $\Lambda^{(j)}$ by the transport relaxation time defined in Eq. (3.17).

The quasiparticle lifetime in the presence of phonon scattering is given by [25]

$$\frac{1}{\tau_{\alpha,\boldsymbol{k}}^{\mathrm{qp}}} = 2\pi \sum_{\alpha',\lambda} \int \frac{d^d q}{(2\pi)^d} |\langle \alpha', \boldsymbol{k}+\boldsymbol{q} | M_\lambda | \alpha, \boldsymbol{k} \rangle|^2$$

$$\times \left\{ \left[ 1 + n_{\mathrm{B}}(\Omega_{\lambda,\boldsymbol{q}}) - f_{\alpha',\boldsymbol{k}+\boldsymbol{q}}^0 \right] \delta(\xi_{\alpha,\boldsymbol{k}} - \xi_{\alpha,\boldsymbol{k}+\boldsymbol{q}} - \Omega_{\lambda,\boldsymbol{q}}) \right.$$

$$\left. + \left[ n_{\mathrm{B}}(\Omega_{\lambda,\boldsymbol{q}}) + f_{\alpha',\boldsymbol{k}+\boldsymbol{q}}^0 \right] \delta(\xi_{\alpha,\boldsymbol{k}} - \xi_{\alpha',\boldsymbol{k}+\boldsymbol{q}} + \Omega_{\lambda,\boldsymbol{q}}) \right\}. \tag{3.28}$$

Here, we replaced $f^0(\xi_{\alpha',\boldsymbol{k}+\boldsymbol{q}})$ by $f_{\alpha',\boldsymbol{k}+\boldsymbol{q}}^0$.

Notably, for phonon emission process $(\xi_{\alpha,\boldsymbol{k}} = \xi_{\alpha',\boldsymbol{k}+\boldsymbol{q}} + \Omega_{\lambda,\boldsymbol{q}})$,

$$1 + n_{\mathrm{B}}(\Omega_{\lambda,\boldsymbol{q}}) - f_{\alpha',\boldsymbol{k}+\boldsymbol{q}}^0 = [1 + n_{\mathrm{B}}(\Omega_{\lambda,\boldsymbol{q}})] \left( \frac{1 - f_{\alpha',\boldsymbol{k}+\boldsymbol{q}}^0}{1 - f_{\alpha,\boldsymbol{k}}^0} \right),$$

$$\tag{3.29}$$

whereas for phonon absorption process $(\xi_{\alpha,\boldsymbol{k}} = \xi_{\alpha',\boldsymbol{k}+\boldsymbol{q}} - \Omega_{\lambda,\boldsymbol{q}})$,

$$n_{\mathrm{B}}(\Omega_{\lambda,\boldsymbol{q}}) + f_{\alpha',\boldsymbol{k}+\boldsymbol{q}}^0 = n_{\mathrm{B}}(\Omega_{\lambda,\boldsymbol{q}}) \left( \frac{1 - f_{\alpha',\boldsymbol{k}+\boldsymbol{q}}^0}{1 - f_{\alpha,\boldsymbol{k}}^0} \right). \tag{3.30}$$

Thus, Eq. (3.28) can be rewritten as

$$\frac{1}{\tau_{\alpha,\boldsymbol{k}}^{\mathrm{qp}}} = \sum_{\alpha'} \int \frac{d^d q}{(2\pi)^d} W_{\alpha',\boldsymbol{k}+\boldsymbol{q};\alpha,\boldsymbol{k}} \left( \frac{1 - f_{\alpha',\boldsymbol{k}+\boldsymbol{q}}^0}{1 - f_{\alpha,\boldsymbol{k}}^0} \right), \tag{3.31}$$

where $W_{\alpha',\boldsymbol{k}+\boldsymbol{q};\alpha,\boldsymbol{k}}$ is the transition rate defined in Eq. (2.14).

Replacing $\Lambda^{(j)}$ by the transport relaxation time and using the definition of quasiparticle lifetime in Eq. (3.31), we can rewrite Eq. (3.27) as

$$\frac{\tau_{\alpha,\boldsymbol{k}}^{(j)}}{\tau_{\alpha,\boldsymbol{k}}^{\mathrm{qp}}} = 1 + \sum_{\alpha'} \int \frac{d^d q}{(2\pi)^d} W_{\alpha',\boldsymbol{k}+\boldsymbol{q};\alpha,\boldsymbol{k}} \frac{v_{\alpha',\boldsymbol{k}+\boldsymbol{q}}^{(j)}}{v_{\alpha,\boldsymbol{k}}^{(j)}} \tau_{\alpha',\boldsymbol{k}+\boldsymbol{q}}^{(j)} \left( \frac{1 - f_{\alpha',\boldsymbol{k}+\boldsymbol{q}}^0}{1 - f_{\alpha,\boldsymbol{k}}^0} \right), \tag{3.32}$$

which is consistent with the semiclassical result in Eq. (2.13).

## 3.3  Ward identities

The validity of the diagrammatic approach in this chapter can be verified by testing the Ward identity [27,28], which is the exact relationship between the self-energy and the

vertex correction arising from the continuity equation. It must hold if the corresponding diagrams are properly included both in the self-energy and the vertex correction. For both elastic and inelastic scatterings, we demonstrate that the Ward identity is satisfied in anisotropic multiband systems as follows:

$$v_{\alpha,\boldsymbol{k}}^{(j)}\Lambda_\alpha^{(j)}(\boldsymbol{k},i\omega_n,i\omega_n) = v_{\alpha,\boldsymbol{k}}^{(j)} + \frac{\partial\Sigma_\alpha(\boldsymbol{k},i\omega_n)}{\partial k^{(j)}}, \tag{3.33}$$

which indicates that we have employed the proper vertex part $\Lambda_\alpha^{(j)}(\boldsymbol{k},i\omega_n,i\omega_n+i\nu_m)$ corresponding to the ladder self-energy diagrams. This can be obtained straightforwardly by subtracting $\Sigma_\alpha(\boldsymbol{k},i\omega_n)$ from $\Sigma_\alpha(\boldsymbol{k}+\boldsymbol{p})$ and taking the limit $\boldsymbol{p}\to 0$ [7].

## 3.4 Alternative derivations for the vertex corrections

In this section, following chapter 10 of Coleman [8], we derive the vertex corrections to the dc conductivity for impurity scattering by performing the momentum integral first. Let us start from Eq. (3.7). The electrons on the Fermi surface mainly contribute to the dc conductivity, and thus we focus on the vertex corrections for electrons at the Fermi energy. As the two Green's functions on the right-hand side of Eq. (3.7) become appreciable near the Fermi energy at low frequencies, we separate the two terms from the rest. Thus, Eq. (3.7) reduces to

$$\Lambda_\alpha^{(j)}(\boldsymbol{k},i\omega_n,i\omega_n+i\nu_m) \approx 1 + n_{\mathrm{imp}}\sum_{\alpha'}\int\frac{d^dk'}{(2\pi)^d}|V_{\alpha',\boldsymbol{k}';\alpha,\boldsymbol{k}}|^2\frac{v_{\alpha',\boldsymbol{k}'}^{(j)}}{v_{\alpha,\boldsymbol{k}}^{(j)}}$$
$$\times \Lambda_{\alpha'}^{(j)}(\boldsymbol{k}',i\omega_n,i\omega_n+i\nu_m)\delta(\xi_{\alpha',\boldsymbol{k}'})$$
$$\times \int d\xi\mathcal{G}(\xi,i\omega_n)\mathcal{G}(\xi,i\omega_n+i\nu_m), \tag{3.34}$$

where

$$\mathcal{G}(\xi,i\omega_n) = \frac{1}{i\omega_n - \xi + i\mathrm{sgn}(\omega_n)\frac{1}{2\tau_{\alpha,\boldsymbol{k}}^{\mathrm{qp}}}} \tag{3.35}$$

is the disorder-averaged Green's function up to the first-order Born approximation. Note that impurity scattering of electrons at the Fermi energy provides a constant con-

tribution to the real part of the self-energy, which can be absorbed in the chemical potential.

First, let us calculate the energy integral. We can compute the energy integral in Eq. (3.34) with the aid of a contour integral method as follows:

$$\int d\xi \mathcal{G}(\xi, i\omega_n)\mathcal{G}(\xi, i\omega_n + i\nu_m) = \frac{2\pi\Theta(\nu_m, \omega_n)}{\nu_m + \frac{1}{\tau_{\alpha',\boldsymbol{k}'}^{\mathrm{qP}}}}, \tag{3.36}$$

where

$$\Theta(\nu_m, \omega_n) = \begin{cases} 1 & \text{for } -\nu_m < \omega_n < 0, \\ 0 & \text{otherwise.} \end{cases} \tag{3.37}$$

Here, we assumed $\nu_m > 0$. Thus, Eq. (3.34) reduces to

$$\Lambda_\alpha^{(j)}(\boldsymbol{k}, i\omega_n, i\omega_n + i\nu_m) \approx 1 + n_{\mathrm{imp}} \sum_{\alpha'} \int \frac{d^d k'}{(2\pi)^d} \delta(\xi_{\alpha',\boldsymbol{k}'}) |V_{\alpha',\boldsymbol{k}';\alpha,\boldsymbol{k}}|^2 \frac{v_{\alpha',\boldsymbol{k}'}^{(j)}}{v_{\alpha,\boldsymbol{k}}^{(j)}}$$
$$\times \Lambda_{\alpha'}^{(j)}(\boldsymbol{k}', i\omega_n, i\omega_n + i\nu_m) \frac{2\pi\Theta(\nu_m, \omega_n)}{\nu_m + \frac{1}{\tau_{\alpha',\boldsymbol{k}'}^{\mathrm{qP}}}}. \tag{3.38}$$

Here, the integral provides a non-zero value only if the poles of the two Green's functions are on the opposite sides with respect to the real axis in frequency space.

Note that, because of the $\Theta(\nu_m, \omega_n)$ term, $\Lambda_\alpha^{(j)}(\boldsymbol{k}, i\omega_n, i\omega_n + i\nu_m)$ has a value independent of $\omega_n$ within the range $-\nu_m < \omega_n < 0$, and otherwise 1. Thus, $\Lambda_\alpha^{(j)}(\boldsymbol{k}, i\omega_n, i\omega_n + i\nu_m)$ can be expressed as

$$\Lambda_\alpha^{(j)}(\boldsymbol{k}, i\omega_n, i\omega_n + i\nu_m) = \begin{cases} \Lambda_\alpha^{(j)}(\boldsymbol{k}, i\nu_m) & \text{for } -\nu_m < \omega_n < 0, \\ 1 & \text{otherwise.} \end{cases} \tag{3.39}$$

Here, we assumed $\Lambda_\alpha^{(j)}(\boldsymbol{k}, i\omega_n, i\omega_n + i\nu_m) = \Lambda_\alpha^{(j)}(\boldsymbol{k}, i\nu_m)$ for $-\nu_m < \omega_n < 0$.

An alternative expression of the dc conductivity in the imaginary time formalism is given by

$$\sigma_{ij}(i\nu_m) = \frac{1}{\nu_m} \left[ \Pi_{ij}(i\nu_m) - \Pi_{ij}(0) \right]. \tag{3.40}$$

Note that electrons near the Fermi surface mostly contribute to the difference between the current-current response functions at $\nu_m$ and $\nu_m = 0$ [8]. Therefore, the dc conductivity can be obtained as

$$
\begin{aligned}
\sigma_{ij}(i\nu_m) &= \frac{ge^2}{\beta\nu_m\mathcal{V}} \sum_{\alpha,\boldsymbol{k},i\omega_n} \Big[ v_{\alpha,\boldsymbol{k}}^{(i)} v_{\alpha,\boldsymbol{k}}^{(j)} \Lambda_\alpha^{(j)}(\boldsymbol{k}, i\omega_n, i\omega_n + i\nu_m) \\
&\quad \times \mathcal{G}_\alpha(\boldsymbol{k}, i\omega_n) \mathcal{G}_\alpha(\boldsymbol{k}, i\omega_n + i\nu_m) - (i\nu_m \to 0) \Big] \\
&\approx \frac{ge^2}{\beta\nu_m} \sum_{\alpha,i\omega_n} \int \frac{d^d k}{(2\pi)^d} \delta(\xi_{\alpha,\boldsymbol{k}}) v_{\alpha,\boldsymbol{k}}^{(i)} v_{\alpha,\boldsymbol{k}}^{(j)} \Big[ \Lambda_\alpha^{(j)}(i\omega_n, i\omega_n + i\nu_m) \\
&\quad \times \int d\xi \mathcal{G}(\xi, i\omega_n) \mathcal{G}(\xi, i\omega_n + i\nu_m) - (i\nu_m \to 0) \Big] \\
&= ge^2 \sum_\alpha \int \frac{d^d k}{(2\pi)^d} \delta(\xi_{\alpha,\boldsymbol{k}}) v_{\alpha,\boldsymbol{k}}^{(i)} v_{\alpha,\boldsymbol{k}}^{(j)} \frac{\Lambda_\alpha^{(j)}(\boldsymbol{k}, i\nu_m)}{\nu_m + \frac{1}{\tau_{\alpha,\boldsymbol{k}}^{\mathrm{qp}}}}.
\end{aligned} \tag{3.41}
$$

Here, we used $\frac{1}{\beta} \sum_{\omega_n} \Theta(\nu_m, \omega_n) = \frac{\nu_m}{2\pi}$. Therefore, by defining the transport relaxation time along the $j$th direction as

$$
\tau_{\alpha,\boldsymbol{k}}^{(j)} \equiv \lim_{\nu_m \to 0} \Lambda_\alpha^{(j)}(\boldsymbol{k}, i\nu_m) \tau_{\alpha,\boldsymbol{k}}^{\mathrm{qp}}, \tag{3.42}
$$

we obtain a result consistent with the dc conductivity obtained through the semiclassical approach in Eq. (2.10).

Performing $\lim_{\nu_m \to 0} \frac{1}{\beta} \sum_{\omega_n} \Theta(\nu_m, \omega_n)$ on both sides of Eq. (3.38), followed by multiplication by $\frac{2\pi}{\nu_m}$, we have

$$
\frac{\tau_{\alpha,\boldsymbol{k}}^{(j)}}{\tau_{\alpha,\boldsymbol{k}}^{\mathrm{qp}}} = 1 + 2\pi n_{\mathrm{imp}} \sum_{\alpha'} \int \frac{d^d k'}{(2\pi)^d} |V_{\alpha',\boldsymbol{k}';\alpha,\boldsymbol{k}}|^2 \delta(\xi_{\alpha,\boldsymbol{k}} - \xi_{\alpha',\boldsymbol{k}'}) \frac{v_{\alpha',\boldsymbol{k}'}^{(j)}}{v_{\alpha,\boldsymbol{k}}^{(j)}} \tau_{\alpha',\boldsymbol{k}'}^{(j)}. \tag{3.43}
$$

Here, we assumed $\xi_{\alpha,\boldsymbol{k}} = \xi_{\alpha',\boldsymbol{k}'} \approx 0$. Therefore, we have an integral equation relating the transport relaxation times as follows:

$$
1 = 2\pi n_{\mathrm{imp}} \sum_{\alpha'} \int \frac{d^d k'}{(2\pi)^d} |V_{\alpha',\boldsymbol{k}';\alpha,\boldsymbol{k}}|^2 \delta(\xi_{\alpha,\boldsymbol{k}} - \xi_{\alpha',\boldsymbol{k}'}) \left( \tau_{\alpha,\boldsymbol{k}}^{(j)} - \frac{v_{\alpha',\boldsymbol{k}'}^{(j)}}{v_{\alpha,\boldsymbol{k}}^{(j)}} \tau_{\alpha',\boldsymbol{k}'}^{(j)} \right), \tag{3.44}
$$

which is consistent with the semiclassical result in Eq. (2.8).

## 3.5   Discussion

In summary, using a diagrammatic approach, we studied the vertex corrections to the dc conductivity in anisotropic multiband systems We demonstrated that the diagrammatic approach provides an equivalent result to that obtained from the semiclassical Boltzmann approach for both elastic and inelastic scatterings. This result provides a many-body justification for the generalized Boltzmann transport theory given by coupled integral equations for anisotropic multiband systems, which is essential to capture the effects of the anisotropy and multiple energy bands on transport correctly.

# Chapter 4

# Quantum interference corrections

In this chapter, we construct a diagrammatic formalism for estimating a quantum interference effect on transport, considering lattice anisotropy and Berry phase effect.

## 4.1 Bethe-Salpeter equation

In the previous chapter, we focused on the ladder vertex corrections combined with the first-order Born approximation, which give the leading impurity correction to the current vertex [Fig. 4.1(a)], satisfying a self-consistent equation [Fig. 4.1(b)]. We demonstrated that this ladder approximation is consistent with the semiclassical Boltzmann transport theory.

To study the quantum interference correction, one should consider further diagrams, called maximally crossed diagrams. The quantum correction can be boiled down to three leading terms referred to as a bare Hikami box and two dressed Hikami boxes [29], as shown in Fig. 4.1(c). The Hikami boxes can be computed by the Cooperon operator, which obeys the following Bethe-Salpeter equation [Fig. 4.1(d)] (in the fol-
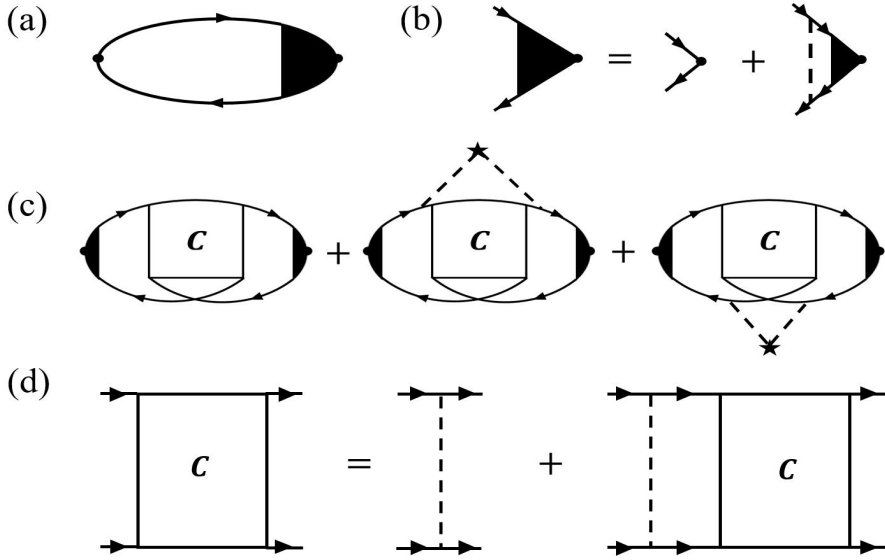
Figure 4.1: Feynman diagrams describing the corrections to the dc conductivity. (a) The current-current correlation function supplemented with the ladder vertex correction gives results equivalent to the Boltzmann transport theory. (b) The ladder vertex correction satisfies the self-consistent Dyson's equation. (c) The quantum correction to the dc conductivity is mostly contributed by a bare Hikami box and two dressed Hikami boxes. (d) The Cooperon operator obeys the self-consistent Bethe-Salpeter equation.

lowing, we omit $\hbar$ for simplicity):

$$C_Q^{\mathrm{AR}}(\boldsymbol{k}, \boldsymbol{k}') = n_{\mathrm{imp}} V_{\boldsymbol{k}',\boldsymbol{k}} V_{-\boldsymbol{k}',-\boldsymbol{k}} \qquad (4.1)$$
$$+ \frac{n_{\mathrm{imp}}}{\mathcal{V}} \sum_{\boldsymbol{p}} V_{\boldsymbol{p},\boldsymbol{k}} V_{-\boldsymbol{p},-\boldsymbol{k}} C_Q^{\mathrm{AR}}(\boldsymbol{p}, \boldsymbol{k}') G^{\mathrm{A}}(\boldsymbol{p}, 0) G^{\mathrm{R}}(\boldsymbol{Q} - \boldsymbol{p}, 0),$$

where $C_Q^{\mathrm{AR}}(\boldsymbol{k}, \boldsymbol{k}')$ is the Cooperon with the momentum $\boldsymbol{Q} = \boldsymbol{k} + \boldsymbol{k}'$, $V_{\boldsymbol{k}',\boldsymbol{k}} = \langle \boldsymbol{k}' | V | \boldsymbol{k} \rangle$ is the matrix element of the scattering potential $V$, and the superscripts A and R represent the advanced and retarded functions, respectively. Here, we assume that $V_{\boldsymbol{Q}-\boldsymbol{k}',\boldsymbol{Q}-\boldsymbol{k}} \approx V_{-\boldsymbol{k}',-\boldsymbol{k}}$ since the Cooperon diverges as $\boldsymbol{Q} \to 0$ and the dominant

contribution comes from small $\boldsymbol{Q}$. We note that frequencies in the Cooperon are set to zero as we focus on the dc conductivity. The retarded and advanced Green's functions are given by $G^{\mathrm{R,A}}(\boldsymbol{p},\xi) = [\xi - \xi_{\boldsymbol{p}} \pm i/2\tau_{\boldsymbol{p}}^{\mathrm{qp}}]^{-1}$. As the Green's functions near the Fermi surface contribute mostly to the momentum summation in the right-hand side of Eq. (4.1), we can perform the $\xi_{\boldsymbol{p}}-$integral separately as $\int d\xi_{\boldsymbol{p}} G^{\mathrm{A}}(\boldsymbol{p},0) G^{\mathrm{R}}(\boldsymbol{Q} - \boldsymbol{p},0) = 2\pi i \left[ \boldsymbol{Q} \cdot \boldsymbol{v_p} + \frac{i}{2} \left( \frac{1}{\tau_{\boldsymbol{p}}^{\mathrm{qp}}} + \frac{1}{\tau_{\boldsymbol{p}-\boldsymbol{Q}}^{\mathrm{qp}}} \right) \right]^{-1}$ [8]. Here, we used $\xi_{\boldsymbol{Q}-\boldsymbol{p}} = \xi_{\boldsymbol{p}-\boldsymbol{Q}} \approx \xi_{\boldsymbol{p}} - \boldsymbol{Q} \cdot \frac{\partial \xi_{\boldsymbol{p}}}{\partial \boldsymbol{p}} = \xi_{\boldsymbol{p}} - \boldsymbol{Q} \cdot \boldsymbol{v_p}$.

We deal with the denominator of Eq. (4.1) using the relation between the self-energy and quasiparticle lifetime, $\Sigma(\boldsymbol{p}) = \lim_{\omega \to 0} \Sigma(\boldsymbol{p}, i\omega_n \to \omega + i0^+) = \frac{-i}{2\tau_{\boldsymbol{p}}^{\mathrm{qp}}}$. Then

$$\frac{i}{2\tau_{\boldsymbol{p}-\boldsymbol{Q}}^{\mathrm{qp}}} = \frac{i}{2\tau_{\boldsymbol{p}}^{\mathrm{qp}}} + \frac{i}{2} \frac{\partial}{\partial \boldsymbol{p}} \left( \frac{1}{\tau_{\boldsymbol{p}}^{\mathrm{qp}}} \right) \cdot (-\boldsymbol{Q}) = \frac{i}{2\tau_{\boldsymbol{p}}^{\mathrm{qp}}} + \boldsymbol{Q} \cdot \frac{\partial \Sigma(\boldsymbol{p})}{\partial \boldsymbol{p}}. \tag{4.2}$$

Using the Ward identity in Eq. (3.33), we have

$$\boldsymbol{Q} \cdot \boldsymbol{v_p} + \frac{i}{2} \left( \frac{1}{\tau_{\boldsymbol{p}}^{\mathrm{qp}}} + \frac{1}{\tau_{\boldsymbol{p}-\boldsymbol{Q}}^{\mathrm{qp}}} \right) = \frac{1}{\tau_{\boldsymbol{p}}^{\mathrm{qp}}} \left( i + \sum_j Q^{(j)} v_{\boldsymbol{p}}^{(j)} \tau_{\boldsymbol{p}}^{(j)} \right). \tag{4.3}$$

Accordingly, the Bethe-Salpeter equation can be rewritten as

$$C_{\boldsymbol{Q}}^{\mathrm{AR}}(\boldsymbol{k}, \boldsymbol{k}') \approx n_{\mathrm{imp}} V_{\boldsymbol{k}', \boldsymbol{k}} V_{-\boldsymbol{k}', -\boldsymbol{k}} \tag{4.4}$$
$$+ \frac{2\pi n_{\mathrm{imp}}}{\mathcal{V}} \sum_{\boldsymbol{p}} \delta(\xi_{\boldsymbol{p}}) V_{\boldsymbol{p}, \boldsymbol{k}} V_{-\boldsymbol{p}, -\boldsymbol{k}} C_{\boldsymbol{Q}}^{\mathrm{AR}}(\boldsymbol{p}, \boldsymbol{k}') \tau_{\boldsymbol{p}}^{\mathrm{qp}} \left[ 1 + i f_{\boldsymbol{Q}}(\boldsymbol{p}) - f_{\boldsymbol{Q}}^2(\boldsymbol{p}) \right],$$

where $f_{\boldsymbol{Q}}(\boldsymbol{p}) \equiv \sum_j Q^{(j)} v_{\boldsymbol{p}}^{(j)} \tau_{\boldsymbol{p}}^{(j)}$. Note that terms of order higher than $Q^2$ are ignored. Importantly, we capture the full anisotropy of the system by introducing $f_{\boldsymbol{Q}}(\boldsymbol{p})$, which is determined by the anisotropic velocities and transport relaxation times on the Fermi surface.

## 4.2   Cooperon ansatz

Now, we are in a position to derive an ansatz of the Bethe-Salpeter equation. We note that there appears $V_{\boldsymbol{k}', \boldsymbol{k}} V_{-\boldsymbol{k}', -\boldsymbol{k}}$ in Eq. (4.4). Let us assume that $V_{-\boldsymbol{k}', -\boldsymbol{k}} \equiv$

$V_{\boldsymbol{k'},\boldsymbol{k}}^* F(\boldsymbol{k}, \boldsymbol{k'})$, where the phase factor $F(\boldsymbol{k}, \boldsymbol{k'})$ depends on the electronic structure of the system. Here, we consider systems where $F(\boldsymbol{k}_1, \boldsymbol{k}_3) = F(\boldsymbol{k}_1, \boldsymbol{k}_2)F(\boldsymbol{k}_2, \boldsymbol{k}_3)$ holds, such as in few-layer black phosphorus. Introducing $\tilde{C}_{\boldsymbol{Q}}^{\mathrm{AR}}(\boldsymbol{k}, \boldsymbol{k'}) \equiv C_{\boldsymbol{Q}}^{\mathrm{AR}}(\boldsymbol{k}, \boldsymbol{k'})F(\boldsymbol{k'}, \boldsymbol{k})$, the Bethe-Salpeter equation reduces to

$$\tilde{C}_{\boldsymbol{Q}}^{\mathrm{AR}}(\boldsymbol{k}, \boldsymbol{k'}) = n_{\mathrm{imp}}|V_{\boldsymbol{k'},\boldsymbol{k}}|^2 \tag{4.5}$$
$$+ \frac{2\pi n_{\mathrm{imp}}}{\mathcal{V}} \sum_{\boldsymbol{p}} \delta(\xi_{\boldsymbol{p}})|V_{\boldsymbol{p},\boldsymbol{k}}|^2 \tilde{C}_{\boldsymbol{Q}}^{\mathrm{AR}}(\boldsymbol{p}, \boldsymbol{k'})\tau_{\boldsymbol{p}}^{\mathrm{qp}} \left[1 + if_{\boldsymbol{Q}}(\boldsymbol{p}) - f_{\boldsymbol{Q}}^2(\boldsymbol{p})\right].$$

Performing $\frac{1}{\mathcal{V}} \sum_{\boldsymbol{k}} \delta(\xi_{\boldsymbol{k}})$ on both sides of Eq. (4.5), we have

$$(2\pi\tau_{\boldsymbol{k'}}^{\mathrm{qp}})^{-1} = \frac{1}{\mathcal{V}} \sum_{\boldsymbol{p}} \delta(\xi_{\boldsymbol{p}})\tilde{C}_{\boldsymbol{Q}}^{\mathrm{AR}}(\boldsymbol{p}, \boldsymbol{k'}) \left[-if_{\boldsymbol{Q}}(\boldsymbol{p}) + f_{\boldsymbol{Q}}^2(\boldsymbol{p})\right], \tag{4.6}$$

where we use the definition of the quasiparticle lifetime $\frac{1}{\tau_{\boldsymbol{p}}^{\mathrm{qp}}} = \frac{2\pi n_{\mathrm{imp}}}{\mathcal{V}} \sum_{\boldsymbol{k}} |V_{\boldsymbol{p},\boldsymbol{k}}|^2 \delta(\xi_{\boldsymbol{k}})$.

Let us consider the following ansatz of Eq. (4.6):

$$\tilde{C}_{\boldsymbol{Q}}^{\mathrm{AR}}(\boldsymbol{k}, \boldsymbol{k'}) = \frac{(2\pi N_0 \tau_{\boldsymbol{k}}^{\mathrm{qp}}\tau_{\boldsymbol{k'}}^{\mathrm{qp}})^{-1}}{\sum_{i,j} D_{ij}Q_iQ_j}, \tag{4.7}$$

where $D_{ij}$ denotes the diffusion coefficients. Plugging this ansatz into Eq. (4.6), we have

$$D_{ij} = \frac{1}{N_0\mathcal{V}} \sum_{\boldsymbol{p}} \delta(\xi_{\boldsymbol{p}})v_{\boldsymbol{p}}^{(i)}v_{\boldsymbol{p}}^{(j)}\tau_{\boldsymbol{p}}^{(i)}\tau_{\boldsymbol{p}}^{(j)}(\tau_{\boldsymbol{p}}^{\mathrm{qp}})^{-1}$$
$$= \frac{1}{N_0\mathcal{V}} \sum_{\boldsymbol{p}} \delta(\xi_{\boldsymbol{p}})(v_{\boldsymbol{p}}^{(i)})^2(\tau_{\boldsymbol{p}}^{(i)})^2(\tau_{\boldsymbol{p}}^{\mathrm{qp}})^{-1}\delta_{ij}. \tag{4.8}$$

Since the most divergent terms in the left and right-hand sides are identical as we plug this ansatz into Eq. (4.5), it is consistent with the ansatz obtained from the iterative method in previous works [30–32]. Finally, we obtain the general ansatz of the Bethe-Salpeter equation as

$$C_{\boldsymbol{Q}}^{\mathrm{AR}}(\boldsymbol{k}, \boldsymbol{k'}) = \frac{(2\pi N_0 \tau_{\boldsymbol{k}}^{\mathrm{qp}}\tau_{\boldsymbol{k'}}^{\mathrm{qp}})^{-1}}{\sum_{i,j} D_{ij}Q_iQ_j} F(\boldsymbol{k}, \boldsymbol{k'}). \tag{4.9}$$

# Chapter 5

# Quantum interference effects in few-layer black phosphorus

In this chapter, using the results of the previous chapter, we study quantum interference effects in few-layer black phosphorus (BP). Few-layer BP is a two-dimensional (2D) van der Waals material, which has been studied intensely both theoretically [14,33–44] and experimentally [45–53]. It is expected to show nontrivial quantum interference effects due to strong anisotropy and tunable electronic structure. Few-layer BP has a direct band gap [Fig. 5.1(a)], which can be tuned by external perturbations, such as strain [33], pressure [49], electric gating [35,41], and chemical doping [37,39]. Such modulations can close the band gap, resulting in the semi-Dirac transition point (SDTP) with a combination of linear and quadratic dispersions [Fig. 5.1(b)]. These modulations can even induce a band inversion, leading to the Dirac semimetal (DSM) phase with linear dispersions around nodes [Fig. 5.1(c)]. Although there have been a few experimental studies on the quantum interference effects in few-layer BP [50–53], a theoretical approach on each phase has been elusive due to its nontrivial anisotropy, which cannot be described by a simple model with different effective masses in each direction. Thus, a further systematic formalism of the quantum interference theory is called for.
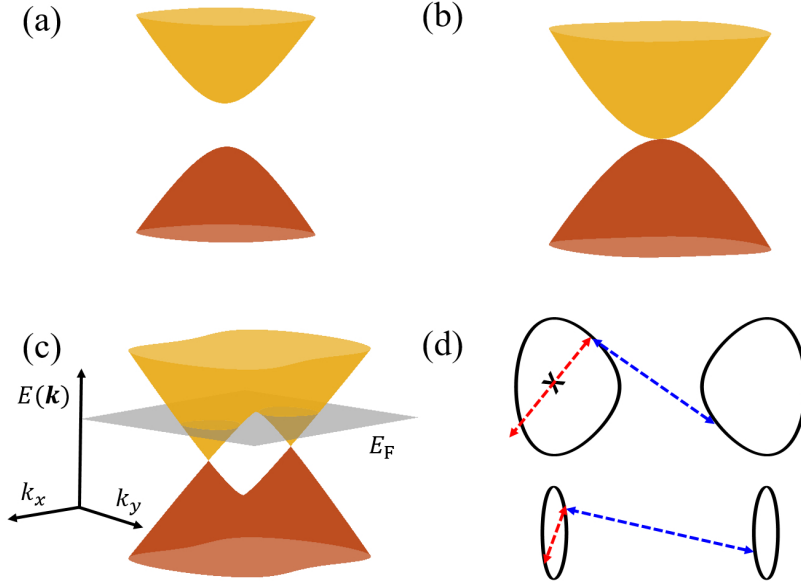
Figure 5.1: Electronic structure of few-layer BP in the (a) insulator phase, (b) semi-Dirac transition point (SDTP), and (c) Dirac semimetal (DSM) phase. (d) The Fermi surfaces of the DSM phase. At a sufficiently low Fermi energy (lower panel), the quantum interference effect is contributed by both of intranode and internode scatterings. As the Fermi energy increases (upper panel), the Fermi surface is distorted and the time-reversal symmetry around a node is broken, and the quantum interference effect via intranode scattering is suppressed.

## 5.1  Model

The low-energy effective Hamiltonian of few-layer BP is given by [14,39,42,44]

$$H = \left( \frac{\hbar^2 k_x^2}{2m^*} + \frac{E_{\mathrm{g}}}{2} \right) \sigma_x + \hbar v_y k_y \sigma_y, \tag{5.1}$$

where $m^*$ is the effective mass along the zigzag $(x)$ direction, $E_{\mathrm{g}}$ is the band gap, $v_y$ is the velocity along the armchair $(y)$ direction, and $\sigma_{x,y}$ are the Pauli matrices. The corresponding energy eigenvalues are given by $E = \pm \sqrt{\left( \frac{\hbar^2 k_x^2}{2m^*} + \frac{E_{\mathrm{g}}}{2} \right)^2 + \hbar^2 v_y^2 k_y^2}$. Without band gap tuning, the Hamiltonian has a direct band gap $(E_{\mathrm{g}} > 0)$ and few-layer BP

29

is in the gapped insulator phase [Fig. 5.1(a)]. At $E_\mathrm{g} = 0$, the Hamiltonian has a band touching point at $(k_x, k_y) = (0, 0)$ and few-layer BP is in the SDTP [Fig. 5.1(b)]. At this point, the energy dispersion is linear in the armchair direction and quadratic in the zigzag direction. As the band gap decreases further to a negative value ($E_\mathrm{g} < 0$), few-layer BP becomes the DSM phase with two nodes at $\boldsymbol{K}^\pm = (\pm\sqrt{\frac{m^*|E_\mathrm{g}|}{\hbar^2}}, 0)$ [Fig. 5.1(c)]. At a sufficiently low Fermi energy satisfying $E_\mathrm{F} \ll |E_\mathrm{g}|$, the Hamiltonian near each node can be linearized as

$$H = \pm\hbar v_x \left(k_x - K_x^\pm\right)\sigma_x + \hbar v_y k_y \sigma_y$$
$$\equiv \hbar v_0 \kappa(\pm\cos\phi_{\boldsymbol{\kappa}}\sigma_x + \sin\phi_{\boldsymbol{\kappa}}\sigma_y), \tag{5.2}$$

where $v_x = \sqrt{\frac{|E_\mathrm{g}|}{m^*}}$ is the velocity along the zigzag direction. For later convenience, we adopt the parametrization $v_0\kappa\cos\phi_{\boldsymbol{\kappa}} = v_x\left(k_x - K_x^\pm\right)$ and $v_0\kappa\sin\phi_{\boldsymbol{\kappa}} = v_y k_y$, where $\boldsymbol{\kappa}$ is an effective momentum measured from the nodes. In this thesis, we neglect the effects of spin-orbit coupling due to its negligible size in few-layer BP.

## 5.2  Weak localization and antilocalization

The quantum correction is determined not only by the electronic structure, but also by the type of impurity. The quantum interference effect is only induced by static and non-magnetic impurities as it is destroyed by non-static or magnetic impurities [4]. Another aspect we should consider is the range of scattering. At low Fermi energies, regardless of the range of scattering, an electron in the insulator phase and SDTP has a single time-reversed counterpart on the whole Fermi surface. In contrast, for the DSM phase we consider two types of scatterings: intranode and internode scatterings [Fig. 5.1(d)]. In the $E_\mathrm{F} \ll E_\mathrm{g}$ limit, intranode scattering may occur by long-range impurities, whereas internode scattering may arise from short-range impurities, such as lattice vacancies. The relative strengths of intranode and internode scatterings lead to competition between the WAL and WL effects in the DSM phase, as will be discussed later.

### 5.2.1 Insulator phase and SDTP

The quantum correction to the dc conductivity is contributed by a bare Hikami box and two dressed Hikami boxes as illustrated in Fig. 4.1(c). Noting the following identities,

$$\int d\xi_{\boldsymbol{k}} |G^{\mathrm{R}}(\boldsymbol{k},0)|^4 = 4\pi(\tau_{\boldsymbol{k}}^{\mathrm{qp}})^3, \tag{5.3a}$$

$$\int d\xi_{\boldsymbol{k}} |G^{\mathrm{R}}(\boldsymbol{k},0)|^2 G^{\mathrm{R}}(\boldsymbol{k},0) = -2\pi i(\tau_{\boldsymbol{k}}^{\mathrm{qp}})^2, \tag{5.3b}$$

we compute the bare Hikami box contribution:

$$
\begin{aligned}
\Delta\sigma_{ii}^{\mathrm{bare}} &\approx \frac{g_s e^2}{2\pi\mathcal{V}^2} \sum_{\boldsymbol{k},\boldsymbol{Q}} |G^{\mathrm{R}}(\boldsymbol{k},0)|^4 C_{\boldsymbol{Q}}^{\mathrm{AR}}(\boldsymbol{k},-\boldsymbol{k}) \tilde{v}_{\boldsymbol{k}}^{(i)} \tilde{v}_{-\boldsymbol{k}}^{(i)} \\
&= -\frac{g_s e^2}{2\pi} \int \frac{d^d k}{(2\pi)^d} \left( v_{\boldsymbol{k}}^{(i)} \frac{\tau_{\boldsymbol{k}}^{(i)}}{\tau_{\boldsymbol{k}}^{\mathrm{qp}}} \right)^2 \delta(\xi_{\boldsymbol{k}}) \int d\xi_{\boldsymbol{k}} |G^{\mathrm{R}}(\boldsymbol{k},0)|^4 \int \frac{d^d Q}{(2\pi)^d} C_{\boldsymbol{Q}}^{\mathrm{AR}}(\boldsymbol{k},-\boldsymbol{k}) \\
&= -\frac{g_s e^2}{\pi N_0} \int \frac{d^d k}{(2\pi)^d} \frac{\left( v_{\boldsymbol{k}}^{(i)} \tau_{\boldsymbol{k}}^{(i)} \right)^2}{\tau_{\boldsymbol{k}}^{\mathrm{qp}}} \delta(\xi_{\boldsymbol{k}}) \int \frac{d^d Q}{(2\pi)^d} \frac{1}{\sum_j D_{jj} Q_j^2}, \tag{5.4}
\end{aligned}
$$

where $g_s = 2$ is the spin degeneracy factor.

Next, let us compute two dressed Hikami boxes, which contribute equally. One of them can be computed as follows:

$$
\begin{aligned}
\Delta\sigma_{ii}^{\mathrm{dressed}} &\approx \frac{g_s e^2}{2\pi\mathcal{V}^3} \sum_{\boldsymbol{k},\boldsymbol{p},\boldsymbol{Q}} n_{\mathrm{imp}} |V_{\boldsymbol{p},\boldsymbol{k}}|^2 |G^{\mathrm{R}}(\boldsymbol{k},0)|^2 G^{\mathrm{R}}(\boldsymbol{k},0) |G^{\mathrm{R}}(\boldsymbol{p},0)|^2 \\
&\quad \times G^{\mathrm{R}}(\boldsymbol{p},0) C_{\boldsymbol{Q}}^{\mathrm{AR}}(\boldsymbol{p},-\boldsymbol{k}) \tilde{v}_{\boldsymbol{k}}^{(i)} \tilde{v}_{-\boldsymbol{p}}^{(i)} \\
&= \frac{g_s e^2}{N_0} \int\int \frac{d^d k}{(2\pi)^d} \frac{d^d p}{(2\pi)^d} n_{\mathrm{imp}} |V_{\boldsymbol{p},\boldsymbol{k}}|^2 v_{\boldsymbol{k}}^{(i)} \tau_{\boldsymbol{k}}^{(i)} v_{\boldsymbol{p}}^{(i)} \tau_{\boldsymbol{p}}^{(i)} \delta(\xi_{\boldsymbol{k}}) \delta(\xi_{\boldsymbol{p}}) \int \frac{d^d Q}{(2\pi)^d} \frac{1}{\sum_j D_{jj} Q_j^2} \\
&= \frac{g_s e^2}{2\pi N_0} \int \frac{d^d p}{(2\pi)^d} \left( v_{\boldsymbol{p}}^{(i)} \frac{\tau_{\boldsymbol{p}}^{(i)}}{\tau_{\boldsymbol{p}}^{\mathrm{qp}}} - v_{\boldsymbol{p}}^{(i)} \right) v_{\boldsymbol{p}}^{(i)} \tau_{\boldsymbol{p}}^{(i)} \delta(\xi_{\boldsymbol{p}}) \int \frac{d^d Q}{(2\pi)^d} \frac{1}{\sum_j D_{jj} Q_j^2} \\
&= -\frac{1}{2}\Delta\sigma_{ii}^{\mathrm{bare}} - \frac{g_s e^2}{2\pi N_0} \int \frac{d^d p}{(2\pi)^d} (v_{\boldsymbol{p}}^{(i)})^2 \tau_{\boldsymbol{p}}^{(i)} \delta(\xi_{\boldsymbol{p}}) \int \frac{d^d Q}{(2\pi)^d} \frac{1}{\sum_j D_{jj} Q_j^2}. \tag{5.5}
\end{aligned}
$$

Therefore, the total quantum correction to the dc conductivity is

$$
\begin{aligned}
\Delta\sigma_{ii} &= \Delta\sigma_{ii}^{\text{bare}} + 2\Delta\sigma_{ii}^{\text{dressed}} \\
&= -\frac{g_s e^2}{\pi N_0} \int \frac{d^d p}{(2\pi)^d} (v_{\boldsymbol{p}}^{(i)})^2 \tau_{\boldsymbol{p}}^{(i)} \delta(\xi_{\boldsymbol{p}}) \int \frac{d^d Q}{(2\pi)^d} \frac{1}{\sum_j D_{jj} Q_j^2},
\end{aligned}
\tag{5.6}
$$

which indicates that the insulator phase and SDTP exhibit the WL effect. To compute the $Q-$integral, let us parametrize the momentum as $\tilde{Q}_x = \sqrt{\frac{D_{xx}}{D}} Q_x$, $\tilde{Q}_y = \sqrt{\frac{D_{yy}}{D}} Q_y$, and $\tilde{Q}^2 = \tilde{Q}_x^2 + \tilde{Q}_y^2$ with $D \equiv \sqrt{D_{xx} D_{yy}}$. Accordingly, the $Q-$integral can be rewritten as

$$
\int \frac{d\tilde{Q}_x d\tilde{Q}_y}{(2\pi)^2} \frac{1}{D(\tilde{Q}_x^2 + \tilde{Q}_y^2)} = \int_{\ell_\phi^{-1}}^{\ell_e^{-1}} \frac{d\tilde{Q}}{(2\pi)} \frac{1}{D\tilde{Q}} = \frac{1}{2\pi D} \ln\left(\frac{\ell_\phi}{\ell_e}\right),
\tag{5.7}
$$

where $\ell_\phi$ is the phase coherence length and $\ell_e$ is the mean-free path. Here, we assume that the lower and upper cutoffs of the integral are given by $\ell_\phi^{-1}$ and $\ell_e^{-1}$, respectively. Restoring $\hbar$, we finally obtain the WL correction as

$$
\Delta\sigma_{ii} = -\frac{1}{2\pi^2 N_0 D\hbar} \ln\left(\frac{\ell_\phi}{\ell_e}\right) \sigma_{ii}^{\text{B}},
\tag{5.8}
$$

where the superscript B denotes the Boltzmann conductivity. This result applies not only to few-layer BP but also to a general 2D anisotropic system. Importantly, the quantum correction is proportional to the Boltzmann conductivity, and thus the ratio of the quantum correction to the Boltzmann conductivity does not depend on the direction regardless of the anisotropy of the system. Rewriting Eq. (5.6) as

$$
\frac{\Delta\sigma_{ii}}{\sigma_{ii}^{\text{B}}} = -\frac{1}{\pi N_0} \int \frac{d^d Q}{(2\pi)^d} \frac{1}{\sum_j D_{jj} Q_j^2},
\tag{5.9}
$$

we note that this direction-independent ratio generally holds even in 3D systems.

### 5.2.2 DSM phase with intranode scattering

For the DSM phase, we compute the quantum corrections due to intranode and internode scatterings, respectively. In this thesis, for simplicity we consider constant intranode and internode scattering potentials given by $V_{\text{intra}}$ and $V_{\text{inter}}$, respectively.

Before studying the quantum interference effect in the DSM phase due to intranode scattering, we note several identities: $N_0 = \frac{g_s E_F}{\pi v_x v_y}$, $(\tau^{\text{qp}})^{-1} = \frac{n_{\text{imp}} V_{\text{intra}}^2 E_F}{2 v_x v_y}$, $(\tau^{\text{tr}})^{-1} = \frac{n_{\text{imp}} V_{\text{intra}}^2 E_F}{4 v_x v_y}$, $D_{xx} = \frac{2 E_F \tau^{\text{qp}}}{N_0 \pi} \left( \frac{v_x}{v_y} \right)$, and $D_{yy} = \frac{2 E_F \tau^{\text{qp}}}{N_0 \pi} \left( \frac{v_y}{v_x} \right)$. Note that the transport relaxation time $\tau^{\text{tr}}$ is isotropic and equals $2\tau^{\text{qp}}$. Using these identities, we obtain the explicit form of the Cooperon as

$$C_{\boldsymbol{Q}}^{\text{AR}}(\boldsymbol{\kappa}, \boldsymbol{\kappa}') = \frac{1}{4(\tau^{\text{qp}})^2} \frac{n_{\text{imp}} V_{\text{intra}}^2 e^{i(\phi - \phi')}}{v_x^2 Q_x^2 + v_y^2 Q_y^2}. \tag{5.10}$$

We note that for backscattering, the phase factor becomes $e^{i(\phi - \phi')} = -1$, and thus the Cooperon has a negative value. Therefore, intranode scattering in the DSM phase induces the WAL effect in the $E_F \ll |E_g|$ limit, as will be demonstrated in the following.

We are now in a position to compute the quantum correction of the DSM phase in the presence of intranode scattering. First, let us compute $\Delta \sigma_{xx}^{\text{bare}}$:

$$\begin{aligned}
\Delta \sigma_{xx}^{\text{bare}} &= \frac{g_s e^2}{\pi N_0} \int \frac{d^d k}{(2\pi)^d} \frac{\left( v_{\boldsymbol{k}}^{(x)} \tau_{\boldsymbol{k}}^{(x)} \right)^2}{\tau_{\boldsymbol{k}}^{\text{qp}}} \delta(\xi_{\boldsymbol{k}}) \int \frac{d^d Q}{(2\pi)^d} \frac{1}{\sum_j D_{jj} Q_j^2} \\
&= \frac{2 g_s e^2}{\pi^2 N_0} \left( \frac{v_x}{v_y} \right) E_F \tau^{\text{qp}} \int \frac{d^d Q}{(2\pi)^d} \frac{1}{\sum_j D_{jj} Q_j^2}. \tag{5.11}
\end{aligned}$$

Next, one of the dressed Hikami boxes reads

$$\begin{aligned}
\Delta \sigma_{xx}^{\text{dressed}} &= -\frac{g_s e^2}{2\pi} \int \int \frac{d^d k}{(2\pi)^d} \frac{d^d k'}{(2\pi)^d} n_{\text{imp}} |V_{\boldsymbol{k}', \boldsymbol{k}}|^2 F(\boldsymbol{k}, \boldsymbol{k}') \left( v_{\boldsymbol{k}}^{(x)} \frac{\tau_{\boldsymbol{k}}^{(x)}}{\tau_{\boldsymbol{k}}^{\text{qp}}} \right) \left( v_{\boldsymbol{k}'}^{(x)} \frac{\tau_{\boldsymbol{k}'}^{(x)}}{\tau_{\boldsymbol{k}'}^{\text{qp}}} \right) \delta(\xi_{\boldsymbol{k}}) \delta(\xi_{\boldsymbol{k}'}) \\
&\quad \times \int d\xi_{\boldsymbol{k}} |G^{\text{R}}(\boldsymbol{k}, 0)|^2 G^{\text{R}}(\boldsymbol{k}, 0) \int d\xi_{\boldsymbol{k}'} |G^{\text{R}}(\boldsymbol{k}', 0)|^2 G^{\text{R}}(\boldsymbol{k}', 0) \int \frac{d^d Q}{(2\pi)^d} C_{\boldsymbol{Q}}^{\text{AR}}(\boldsymbol{k}', -\boldsymbol{k}) \\
&= -\frac{g_s e^2}{2\pi^2 N_0} \left( \frac{v_x}{v_y} \right) E_F \tau^{\text{qp}} \int \frac{d^d Q}{(2\pi)^d} \frac{1}{\sum_j D_{jj} Q_j^2} = -\frac{1}{4} \Delta \sigma_{xx}^{\text{bare}}. \tag{5.12}
\end{aligned}$$

Accordingly, the total quantum correction to the dc conductivity is

$$\begin{aligned}
\Delta \sigma_{xx} &= \Delta \sigma_{xx}^{\text{bare}} + 2 \Delta \sigma_{xx}^{\text{dressed}} = \frac{1}{2} \Delta \sigma_{xx}^{\text{bare}} \\
&= \frac{g_s e^2}{\pi^2 N_0} \left( \frac{v_x}{v_y} \right) E_F \tau^{\text{qp}} \int \frac{d^d Q}{(2\pi)^d} \frac{1}{\sum_j D_{jj} Q_j^2}. \tag{5.13}
\end{aligned}$$

33

The $Q-$integral can be computed by introducing $\tilde{Q}_x = \sqrt{\frac{D_{xx}}{D}} Q_x$ and $\tilde{Q}_y = \sqrt{\frac{D_{yy}}{D}} Q_y$ with $D = \sqrt{D_{xx}D_{yy}}$, similarly as we did for the insulator phase and SDTP:

$$\int_{\ell_\phi^{-1}}^{\ell_{\mathrm{intra}}^{-1}} \frac{d\tilde{Q}}{(2\pi)} \frac{1}{d\tilde{Q}} = \frac{1}{2\pi D} \ln\left(\frac{\ell_\phi}{\ell_{\mathrm{intra}}}\right) = \frac{N_0}{4E_{\mathrm{F}}\tau^{\mathrm{qp}}} \ln\left(\frac{\ell_\phi}{\ell_{\mathrm{intra}}}\right), \tag{5.14}$$

where $\ell_{\mathrm{intra}}$ is the mean-free path corresponding to intranode scattering. Restoring $\hbar$, we obtain the total quantum correction to the dc conductivity as

$$\Delta\sigma_{xx} = \frac{g_s e^2}{4\pi^2 \hbar} \left(\frac{v_x}{v_y}\right) \ln\left(\frac{\ell_\phi}{\ell_{\mathrm{intra}}}\right), \tag{5.15a}$$

$$\Delta\sigma_{yy} = \frac{g_s e^2}{4\pi^2 \hbar} \left(\frac{v_y}{v_x}\right) \ln\left(\frac{\ell_\phi}{\ell_{\mathrm{intra}}}\right), \tag{5.15b}$$

or equivalently

$$\Delta\sigma_{ii} = \frac{n_{\mathrm{imp}} V_{\mathrm{intra}}^2}{8\pi\hbar^2 v_x v_y} \ln\left(\frac{\ell_\phi}{\ell_{\mathrm{intra}}}\right) \sigma_{ii}^{\mathrm{B}}, \tag{5.16}$$

where $\sigma_{ii}^{\mathrm{B}} = \frac{2g_s e^2 v_i^2 \hbar}{\pi n_{\mathrm{imp}} V_{\mathrm{intra}}^2}$ is the Boltzmann conductivity along the $i$th direction. Note that the ratio $\Delta\sigma_{ii}/\sigma_{ii}^{\mathrm{B}}$ is the same irrespective of the direction.

### 5.2.3 DSM phase with internode scattering

Using the eigenstates in the DSM phase, we can obtain the matrix elements for internode scattering as

$$V_{\boldsymbol{\kappa}',\boldsymbol{\kappa}}^{+,-} = \frac{V_{\mathrm{inter}}}{2}[1 - e^{-i(\phi+\phi')}], \tag{5.17a}$$

$$V_{-\boldsymbol{\kappa}',-\boldsymbol{\kappa}}^{-,+} = \frac{V_{\mathrm{inter}}}{2}[1 - e^{i(\phi+\phi')}], \tag{5.17b}$$

where $V_{\mathrm{inter}}$ is internode scattering amplitude, and the superscripts $+$ and $-$ denote the positive and negative nodes, respectively. Thus, $V_{\boldsymbol{\kappa}',\boldsymbol{\kappa}}^{+,-} V_{-\boldsymbol{\kappa}',-\boldsymbol{\kappa}}^{-,+} = |V_{\boldsymbol{\kappa}',\boldsymbol{\kappa}}^{+,-}|^2$ and we have the Cooperon ansatz as

$$C_{\boldsymbol{Q}}^{\mathrm{AR}}(\boldsymbol{\kappa},\boldsymbol{\kappa}') = \frac{(2\pi N_0 \tau_{\boldsymbol{\kappa}}^{\mathrm{qp}} \tau_{\boldsymbol{\kappa}'}^{\mathrm{qp}})^{-1}}{\sum_{i,j} D_{ij} Q_i Q_j}. \tag{5.18}$$

Repeating the steps in the previous section, we obtain the quantum correction due to internode scattering as

$$\Delta\sigma_{xx} = -\frac{g_s e^2}{4\pi^2 \hbar} \left( \frac{v_x}{v_y} \right) \ln \left( \frac{\ell_\phi}{\ell_{\text{inter}}} \right), \tag{5.19a}$$

$$\Delta\sigma_{yy} = -\frac{g_s e^2}{4\pi^2 \hbar} \left( \frac{v_y}{v_x} \right) \ln \left( \frac{\ell_\phi}{\ell_{\text{inter}}} \right), \tag{5.19b}$$

or equivalently

$$\Delta\sigma_{ii} = -\frac{n_{\text{imp}} V_{\text{inter}}^2}{8\pi \hbar^2 v_x v_y} \ln \left( \frac{\ell_\phi}{\ell_{\text{inter}}} \right) \sigma_{ii}^{\text{B}}, \tag{5.20}$$

which differs only by the sign from the quantum correction for intranode scattering in Eq. (5.16) with $\ell_{\text{intra}}$ ($V_{\text{intra}}$) replaced by $\ell_{\text{inter}}$ ($V_{\text{inter}}$). Note that as for the intranode scattering, the ratio $\Delta\sigma_{ii}/\sigma_{ii}^{\text{B}}$ is the same irrespective of the direction.

In the presence of both intranode and internode scatterings, the quantum interference effect in the DSM phase is determined by the dominant scattering process. Thus, we expect that the WAL (WL) effect will occur when intranode (internode) scattering is dominant.

## 5.3   Magnetoconductivity

Applying an external magnetic field gives an additional phase to each backscattering path, and thus destroys the quantum interference effect [3,4]. In experiments, the phase coherence length can be obtained through the measurement of magnetoconductivity. In the following, we compute the magnetoconductivity of each phase using the quantization of Landau levels [4,32].

### 5.3.1   Insulator phase

In the following, we restore $\hbar$ for clarity. According to J. M. Pereira, Jr *et al.* [38], the Landau levels in small $B$ have a linear dependence on magnetic field, as in the case of a free electron gas. Thus, for the insulator phase, we adopt the Hamiltonian of an anisotropic free electron gas as $H = \frac{p_x^2}{2m_x} + \frac{p_y^2}{2m_y}$ with effective masses $m_{x,y}$ along

each direction. The corresponding Landau levels are given by $E_n = \frac{\hbar e B}{\sqrt{m_x m_y} c} \left( n + \frac{1}{2} \right)$. Since the ratio between the diffusion coefficients are given by $\frac{D_{xx}}{D_{yy}} = \frac{m_y}{m_x}$, the Landau quantization of momentum reads

$$D_{xx} Q_{n,x}^2 + D_{yy} Q_{n,y}^2 = \frac{D}{\ell_B^2} \left( n + \frac{1}{2} \right). \tag{5.21}$$

Here, we define the magnetic length $\ell_B = \sqrt{\frac{\hbar c}{4eB}}$. Following the above quantization condition, we modify the $Q-$integral in Eq. (5.6) by

$$\sum_n \int \frac{d^2 Q}{(2\pi)^2} \frac{1}{D_{xx} Q_x^2 + D_{yy} Q_y^2} \delta \left[ n + \frac{1}{2} - \frac{\ell_B^2}{D} (D_{xx} Q_x^2 + D_{yy} Q_y^2) \right]$$

$$= \sum_n \int \frac{d\tilde{Q}_x d\tilde{Q}_y}{(2\pi)^2 D \tilde{Q}^2} \delta \left( n + \frac{1}{2} - \ell_B^2 \tilde{Q}^2 \right) = \frac{1}{4\pi D} \sum_{n_{\min}}^{n_{\max}} \frac{1}{n + \frac{1}{2}}, \tag{5.22}$$

where $n_{\min} = (\ell_B \ell_\phi^{-1})^2$ and $n_{\max} = (\ell_B \ell_e^{-1})^2$. Thus, the $Q-$integral can be rewritten in terms of the digamma function $\Psi(x)$ as

$$\frac{1}{4\pi D} \left[ \Psi \left( \frac{1}{2} + \frac{\ell_B^2}{\ell_e^2} \right) - \Psi \left( \frac{1}{2} + \frac{\ell_B^2}{\ell_\phi^2} \right) \right], \tag{5.23}$$

where we used $\Psi(x + N) - \Psi(x) = \sum_{k=0}^{N-1} \frac{1}{x+k}$. Accordingly, we obtain the magnetoconductivity of the insulator phase as

$$\Delta \sigma_{ii}(B) = -\frac{g_s e^2}{4\pi^2 N_0 D \hbar} \left[ \Psi \left( \frac{1}{2} + \frac{\ell_B^2}{\ell_e^2} \right) - \Psi \left( \frac{1}{2} + \frac{\ell_B^2}{\ell_\phi^2} \right) \right] \int \frac{d^d p}{(2\pi)^d} [v_{\boldsymbol{p}}^{(i)}]^2 \tau_{\boldsymbol{p}}^{(i)} \delta(\xi_{\boldsymbol{p}}). \tag{5.24}$$

Since the digamma function follows the asymptotic form $\Psi \left( \frac{1}{2} + x \right) \approx \ln x + \frac{1}{24x^2} + \cdots$ for $x \to \infty$, the magnetoconductivity reduces to Eq. (5.8) in the $B \to 0$ limit. Thus, the ratio between the magnetoconductivity [Eq. (5.24)] and the dc conductivity [Eq. (3.15)] reads

$$\frac{\Delta \sigma_{ii}(B) - \Delta \sigma_{ii}(0)}{\sigma_{ii}^{\mathrm{B}}} = -\frac{1}{4\pi^2 N_0 D \hbar} \left[ \Psi \left( \frac{1}{2} + \frac{\ell_B^2}{\ell_e^2} \right) - \Psi \left( \frac{1}{2} + \frac{\ell_B^2}{\ell_\phi^2} \right) - 2 \ln \left( \frac{\ell_\phi}{\ell_e} \right) \right]. \tag{5.25}$$

Again, the ratio is irrespective of the direction.

### 5.3.2 DSM phase

Now, let us consider the DSM phase. Applying an external magnetic field perpendicular to the $xy$ plane, say $\boldsymbol{B} = (0, 0, B)$, the crystal momentum is transformed as $\hbar \boldsymbol{k} = \boldsymbol{p} + \frac{e}{c}\boldsymbol{A}$ where $\boldsymbol{p}$ is the canonical momentum and $\boldsymbol{A}$ is the vector potential. Thus, the Hamiltonian becomes

$$H = v_x p_x \sigma_x + v_y \left( p_y + \frac{eBx}{c} \right) \sigma_y, \tag{5.26}$$

where we chose the Landau gauge $\boldsymbol{A} = (0, Bx, 0)$ for the vector potential. Then we have the $n$th Landau level as

$$E_n^2 = v_x^2 p_x^2 + v_y^2 \left( p_y + \frac{eBx}{c} \right)^2 - \frac{\hbar e B v_x v_y}{c} = \frac{2\hbar e B v_x v_y n}{c}. \tag{5.27}$$

Note that the momentum along the $y$ axis is a good quantum number. Thus, the crystal momentum follows the quantization $\hbar^2 v_x^2 k_x^2 + \hbar^2 v_y^2 k_y^2 = v_x^2 p_x^2 + v_y^2 \left( p_y + \frac{eBx}{c} \right)^2 = \frac{2\hbar e B v_x v_y}{c} \left( n + \frac{1}{2} \right)$. The quantization for $\boldsymbol{Q} = \boldsymbol{k} + \boldsymbol{k}'$ is obtained by doubling the magnetic field:

$$v_x^2 Q_{n,x}^2 + v_y^2 Q_{n,y}^2 = \frac{4eB}{\hbar c} v_x v_y \left( n + \frac{1}{2} \right), \tag{5.28}$$

which is equivalent to Eq. (5.21) in the insulator phase. Therefore, we compute the magnetoconductivity in the DSM phase in a similar manner as in the insulator phase:

$$\Delta\sigma_{xx}(B) = \frac{g_s e^2}{8\pi^2 \hbar} \left( \frac{v_x}{v_y} \right) \left[ \Psi \left( \frac{1}{2} + \frac{\ell_B^2}{\ell_{\text{intra}}^2} \right) - \Psi \left( \frac{1}{2} + \frac{\ell_B^2}{\ell_\phi^2} \right) \right], \tag{5.29a}$$

$$\Delta\sigma_{yy}(B) = \frac{g_s e^2}{8\pi^2 \hbar} \left( \frac{v_y}{v_x} \right) \left[ \Psi \left( \frac{1}{2} + \frac{\ell_B^2}{\ell_{\text{intra}}^2} \right) - \Psi \left( \frac{1}{2} + \frac{\ell_B^2}{\ell_\phi^2} \right) \right], \tag{5.29b}$$

or equivalently

$$\begin{aligned}
\frac{\Delta\sigma_{ii}(B) - \Delta\sigma_{ii}(0)}{\sigma_{ii}^{\text{B}}} &= \frac{n_{\text{imp}} V_{\text{intra}}^2}{16\pi\hbar^2 v_x v_y} \left[ \Psi \left( \frac{1}{2} + \frac{\ell_B^2}{\ell_{\text{intra}}^2} \right) - \Psi \left( \frac{1}{2} + \frac{\ell_B^2}{\ell_\phi^2} \right) - 2\ln \left( \frac{\ell_\phi}{\ell_{\text{intra}}} \right) \right] \\
&= \frac{\hbar}{8\pi E_F \tau_{\text{intra}}^{\text{qp}}} \left[ \Psi \left( \frac{1}{2} + \frac{\ell_B^2}{\ell_{\text{intra}}^2} \right) - \Psi \left( \frac{1}{2} + \frac{\ell_B^2}{\ell_\phi^2} \right) - 2\ln \left( \frac{\ell_\phi}{\ell_{\text{intra}}} \right) \right].
\end{aligned} \tag{5.30}$$

We note that in the $B \to 0$ limit, Eqs. (5.29a) and (5.29b) reduce to Eq. (5.15a) and (5.15b), respectively. Similarly, we can compute the magnetoconductivity for internode scattering, which only differs from the result in Eq. (5.30) by the sign, with $\ell_{\text{intra}}$ ($\tau_{\text{intra}}^{\text{qp}}$) replaced by $\ell_{\text{inter}}$ ($\tau_{\text{inter}}^{\text{qp}}$).

### 5.3.3  SDTP

Following Petra Dietl *et al.* [54], we have the Landau quantization for the momentum $\boldsymbol{Q}$ at the SDTP as follows:

$$\frac{\hbar^4 Q_x^4}{4m^{*2}} + \hbar^2 v_y^2 Q_y^2 = A^2 \left(\frac{\hbar}{2\ell_B^2}\right)^{\frac{4}{3}} \left(\frac{v_y^2}{m^*}\right)^{\frac{2}{3}} \left(n + \frac{1}{2}\right)^{\frac{4}{3}}, \tag{5.31}$$

where $A \approx 1.17325$. Considering the Landau quantization, we rewrite the $Q-$integral in Eq. (5.6) for the quantum correction as

$$\sum_n \int \frac{dQ_x dQ_y}{(2\pi)^2} \frac{1}{D_{xx}Q_x^2 + D_{yy}Q_y^2} \delta \left[n + \frac{1}{2} - \left(\frac{\hbar^4 Q_x^4}{4m^{*2}} + \hbar^2 v_y^2 Q_y^2\right)^{\frac{3}{4}} \times \frac{\sqrt{m^*}}{v_y} \frac{2\ell_B^2}{\hbar^2 A^{\frac{3}{2}}}\right] \tag{5.32}$$

The momentum $\tilde{Q} = \sqrt{\tilde{Q}_x^2 + \tilde{Q}_y^2}$ is bounded as $\ell_\phi^{-1} \le \tilde{Q} \le \ell_e^{-1}$. We rewrite the $Q-$integral as

$$\sum_n \int \frac{d\tilde{Q}_x d\tilde{Q}_y}{(2\pi)^2 D} \frac{1}{\tilde{Q}_x^2 + \tilde{Q}_y^2} \delta \left[n + \frac{1}{2} - \left(\frac{\hbar^4 \tilde{Q}_x^4}{4m^{*2}} \left(\frac{D}{D_{xx}}\right)^2 + \alpha \hbar^2 v_y^2 \tilde{Q}_y^2 \left(\frac{D}{D_{yy}}\right)\right)^{\frac{3}{4}}\right] \tag{5.33}$$

where $\alpha \equiv \frac{\sqrt{m^*}}{v_y} \frac{2\ell_B^2}{\hbar^2 A^{\frac{3}{2}}}$. Note that we consider the region where $\tilde{Q}_x$ and $\tilde{Q}_y$ are positive. To calculate the $Q_y-$integral first, we transform the delta function in Eq. (5.33) into

$$\frac{\delta \left[\tilde{Q}_y - \frac{1}{\hbar v_y} \sqrt{\frac{D_{yy}}{D}} \sqrt{\frac{1}{\alpha^{\frac{4}{3}}} \left(n + \frac{1}{2}\right)^{\frac{4}{3}} - \frac{\hbar^4 \tilde{Q}_x^4}{4m^{*2}} \left(\frac{D}{D_{xx}}\right)^2}\right]}{\frac{3\alpha}{4} \left[\frac{\hbar^4 \tilde{Q}_x^4}{4m^{*2}} \left(\frac{D}{D_{xx}}\right)^2 + \hbar^2 v_y^2 \tilde{Q}_y^2 \left(\frac{D}{D_{yy}}\right)\right]^{-\frac{1}{4}} \times \hbar^2 v_y^2 \frac{D}{D_{yy}} \times 2\tilde{Q}_y}. \tag{5.34}$$

We deal with the above integral differently based on the region $\tilde{Q}_x$ lies in: 1) $\ell_\phi^{-1} \le |\tilde{Q}_x| \le \ell_e^{-1} : 0 \le |\tilde{Q}_y| \le \sqrt{\ell_e^{-2} - \tilde{Q}_x^2}$, 2) $|\tilde{Q}_x| \le \ell_\phi^{-1} : \sqrt{\ell_\phi^{-2} - \tilde{Q}_x^2} \le |\tilde{Q}_y| \le$

$\sqrt{\ell_e^{-2} - \tilde{Q}_x^2}$. Ignoring terms of order higher than $\tilde{Q}_x^2$, we rewrite Eq. (5.33) as

$$\sum_{n_{min}^{(1)}}^{n_{max}^{(1)}} \int_{\ell_\phi^{-1}}^{\ell_e^{-1}} \frac{d\tilde{Q}_x}{(2\pi)^2 D} \frac{4}{3\alpha} \frac{1}{2\hbar v_0} \sqrt{\frac{D_{yy}}{D}} \times \left( \frac{1}{\tilde{Q}_x^2 + \frac{D_{yy}}{\hbar^2 v_y^2 D} \left(n + \frac{1}{2}\right)^{\frac{4}{3}} \frac{1}{\alpha^{\frac{4}{3}}}} \right) \times \frac{4}{\left(n + \frac{1}{2}\right)^{\frac{1}{3}} \frac{1}{\alpha^{\frac{1}{3}}}}$$

$$+ \sum_{n_{min}^{(2)}}^{n_{max}^{(2)}} \int_0^{\ell_\phi^{-1}} \frac{d\tilde{Q}_x}{(2\pi)^2 D} \frac{4}{3\alpha} \frac{1}{2\hbar v_0} \sqrt{\frac{D_{yy}}{D}} \times \left( \frac{1}{\tilde{Q}_x^2 + \frac{D_{yy}}{\hbar^2 v_y^2 D} \left(n + \frac{1}{2}\right)^{\frac{4}{3}} \frac{1}{\alpha^{\frac{4}{3}}}} \right) \times \frac{4}{\left(n + \frac{1}{2}\right)^{\frac{1}{3}} \frac{1}{\alpha^{\frac{1}{3}}}}.$$

$$(5.35)$$

Note that 1) $n_{min}^{(1)} = 0$, $n_{max}^{(1)} = \alpha \left[ \hbar^2 v_y^2 \left( \frac{D}{D_{yy}} \right) (\ell_e^{-2} - \tilde{Q}_x^2) \right]^{\frac{3}{4}} - \frac{1}{2}$, and 2) $n_{min}^{(2)} = \alpha \left[ \hbar^2 v_y^2 \left( \frac{D}{D_{yy}} \right) (\ell_\phi^{-2} - \tilde{Q}_x^2) \right]^{\frac{3}{4}} - \frac{1}{2}$, $n_{max}^{(2)} = \alpha \left[ \hbar^2 v_y^2 \left( \frac{D}{D_{yy}} \right) (\ell_e^{-2} - \tilde{Q}_x^2) \right]^{\frac{3}{4}} - \frac{1}{2}$.

We replace the $n-$sum by the $n-$integral as follows:

$$\frac{2\hbar v_y}{3\pi^2 D} \sqrt{\frac{D}{D_{yy}}} \alpha^{\frac{2}{3}} \left[ \int_{\ell_\phi^{-1}}^{\ell_e^{-1}} d\tilde{Q}_x \int_{\frac{1}{2}}^{n_{max}^{(1)} + \frac{1}{2}} dn \frac{1}{n^{\frac{5}{3}} + \left( \alpha^{\frac{4}{3}} \tilde{Q}_x^2 \frac{D}{D_{yy}} \hbar^2 v_y^2 \right) n^{\frac{1}{3}}} \right. \qquad (5.36)$$

$$\left. + \int_0^{\ell_\phi^{-1}} d\tilde{Q}_x \int_{n_{min}^{(2)} + \frac{1}{2}}^{n_{max}^{(2)} + \frac{1}{2}} dn \frac{1}{n^{\frac{5}{3}} + \left( \alpha^{\frac{4}{3}} \tilde{Q}_x^2 \frac{D}{D_{yy}} \hbar^2 v_y^2 \right) n^{\frac{1}{3}}} \right].$$

One can check the validity of this replacement by applying it to Eq. (5.22), giving the consistent result. Now, let us introduce $\gamma = \alpha^{\frac{4}{3}} \tilde{Q}_x^2 \frac{D}{D_{yy}} \hbar^2 v_y^2$. The $n-$integral can be computed by the following indefinite integral:

$$\int dn \frac{1}{n^{\frac{5}{3}} + \gamma n^{\frac{1}{3}}} = \frac{3}{2\sqrt{\gamma}} \tan^{-1} \left( \frac{n^{\frac{2}{3}}}{\sqrt{\gamma}} \right) + C. \qquad (5.37)$$

Accordingly, Eq. (5.36) can be rewritten as

$$\frac{1}{\pi^2 D} \left[ \int_0^{\ell_e^{-1}} d\tilde{Q}_x \frac{1}{\tilde{Q}_x} \tan^{-1} \left( \frac{\sqrt{\ell_e^{-2} - \tilde{Q}_x^2}}{\tilde{Q}_x} \right) - \int_0^{\ell_\phi^{-1}} d\tilde{Q}_x \frac{1}{\tilde{Q}_x} \tan^{-1} \left( \frac{\sqrt{\ell_\phi^{-2} - \tilde{Q}_x^2}}{\tilde{Q}_x} \right) \right]$$

$$- \frac{1}{\pi^2 D} \int_{\ell_\phi^{-1}}^{\ell_e^{-1}} d\tilde{Q}_x \frac{1}{\tilde{Q}_x} \tan^{-1} \left( \frac{\alpha^{-\frac{2}{3}}}{2^{\frac{2}{3}} \tilde{Q}_x \hbar v_y} \sqrt{\frac{D_{yy}}{D}} \right). \qquad (5.38)$$

Since the first and second terms in Eq. (5.38) are $B-$independent, the magnetoconductivity is only contributed by the third term. Finally, we obtain the ratio between the

magnetoconductivity and the Boltzmann conductivity at the SDTP as

$$\frac{\Delta\sigma_{ii}(B) - \Delta\sigma_{ii}(0)}{\sigma_{ii}^{\mathrm{B}}} = \frac{1}{\pi^3 D N_0 \hbar} \int_{\ell_\phi^{-1}}^{\ell_e^{-1}} d\tilde{Q}_x \frac{1}{\tilde{Q}_x} \tan^{-1}\left(\frac{\alpha^{-\frac{2}{3}}}{2^{\frac{2}{3}}\tilde{Q}_x \hbar v_y}\sqrt{\frac{D_{yy}}{D}}\right).(5.39)$$

Note that the ratio is also independent of the direction. Eq. (5.39) indicates the $B^{2/3}$ dependence of the magnetoconductivity in the weak field limit ($\ell_\phi \ll \ell_B$). As for the intermediate field regime ($\ell_e \leq \ell_B \ll \ell_\phi$), we predict that the magnetoconductivity will follow the power-law dependence on $B$ with the exponent $\nu$, which may vary depending on the system parameter.

## 5.4 Discussion
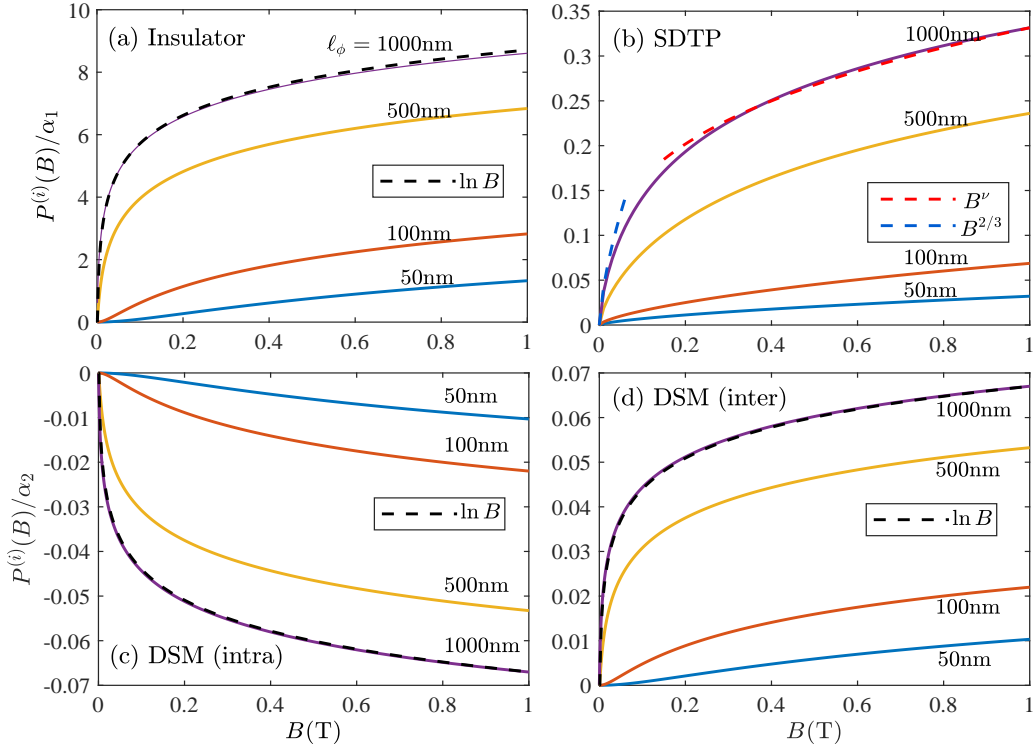


Figure 5.2: Ratio of the field-induced change in the magnetoconductivity to the Boltzmann conductivity for various phase coherence lengths with $\ell_e = 10$nm. The ratio for the WL correction in (a) the insulator phase and (b) SDTP are plotted in units of $\alpha_1 = n_{\text{imp}}V_{\text{imp}}^2/\hbar^2 v_y^2$. As for the DSM phase, intranode and internode scatterings induce (c) WAL and (d) WL, respectively. Both corrections are plotted in units of $\alpha_2 = n_{\text{imp}}V_{\text{imp}}^2/\hbar^2 v_x v_y$. The black dashed lines denote the $\pm \ln B$ dependence, while the red dashed line and blue dashed line in (b) represent the $B^\nu$ dependence with $\nu \approx 0.31$ and $B^{2/3}$ dependence, respectively.

In summary, we obtain the ratio $P^{(i)}(B) \equiv [\Delta\sigma_{ii}(B) - \Delta\sigma_{ii}(0)]/\sigma_{ii}^{\mathrm{B}}$ for each phase as follows:

$$P_{\mathrm{ins}}^{(i)}(B) = -\frac{1}{4\pi^2 N_0 D\hbar}\left[\Psi\left(\frac{1}{2} + \frac{\ell_B^2}{\ell_e^2}\right) - \Psi\left(\frac{1}{2} + \frac{\ell_B^2}{\ell_\phi^2}\right) - 2\ln\left(\frac{\ell_\phi}{\ell_e}\right)\right], \quad (5.40a)$$

$$P_{\mathrm{SDTP}}^{(i)}(B) = \frac{1}{\pi^3 D N_0 \hbar}\int_{\ell_\phi^{-1}}^{\ell_e^{-1}} d\tilde{Q}_x \frac{1}{\tilde{Q}_x}\tan^{-1}\left(\frac{\alpha^{-\frac{2}{3}}}{2^{\frac{2}{3}}\tilde{Q}_x \hbar v_y}\sqrt{\frac{D_{yy}}{D}}\right), \quad (5.40b)$$

$$P_{\mathrm{DSM}}^{(i)}(B) = \frac{\hbar}{8\pi E_{\mathrm{F}}\tau_{\mathrm{intra}}^{\mathrm{qp}}}\left[\Psi\left(\frac{1}{2} + \frac{\ell_B^2}{\ell_{\mathrm{intra}}^2}\right) - \Psi\left(\frac{1}{2} + \frac{\ell_B^2}{\ell_\phi^2}\right) - 2\ln\left(\frac{\ell_\phi}{\ell_{\mathrm{intra}}}\right)\right],$$

$$(5.40c)$$

where $\Psi(x)$ is the digamma function, $\alpha \equiv \frac{\sqrt{m^*}}{v_y}\frac{2\ell_B^2}{\hbar^2 A^{\frac{3}{2}}}$ with $A \approx 1.17325$ [54] and $\ell_B = \sqrt{\frac{\hbar c}{4eB}}$ is the magnetic length. Eq. (5.40c) is obtained for intranode scattering, and the field-dependence for internode scattering only differs by the sign, with $\ell_{\mathrm{intra}}$ ($\tau_{\mathrm{intra}}^{\mathrm{qp}}$) replaced by $\ell_{\mathrm{inter}}$ ($\tau_{\mathrm{inter}}^{\mathrm{qp}}$).

For the insulator phase [Fig. 5.2(a)] and DSM phase [Figs. 5.2(c) and 5.2(d)], we find that the field-dependence of the magnetoconductivity is well approximated by $P^{(i)}(B) \propto \pm\ln B$, which is in good agreement with the conventional prediction for 2D systems [2]. However, we predict that the magnetoconductivity of the SDTP will not follow the conventional prediction, but rather will show $P^{(i)}(B) \propto B^{\frac{2}{3}}$ dependence in the weak field limit ($\ell_\phi \ll \ell_B$), whereas $P^{(i)}(B) \propto B^\nu$ dependence in the intermediate field regime ($\ell_e \leq \ell_B \ll \ell_\phi$) with the exponent $\nu$, which depends on the system parameter and can be found numerically. This nontrivial field-dependence may be attributed to strong anisotropy in the band dispersion [5], leading to a quantum diffusion which deviates from the 2D behavior. We note that $P^{(i)}(B)$, the ratio of the field-induced change in the magnetoconductivity to the Boltzmann conductivity, is the same irrespective of the direction $i$ for each phase.

Our analysis shows that the sign of the quantum correction is determined by the electronic structure-dependent phase factor $F(\boldsymbol{k}, \boldsymbol{k}')$, which reflects the symmetry class of the system [30, 55, 56]. The unity phase factor of the insulator phase and SDTP indicates that the system has spinless time-reversal symmetry, belonging to the

orthogonal class. Backscattering induced by a time-reversal operator of this kind leads to WL. As for the DSM phase, in the absence of internode scattering, the phase factor $F(\boldsymbol{\kappa}, \boldsymbol{\kappa}') = e^{i(\phi_{\boldsymbol{\kappa}} - \phi_{\boldsymbol{\kappa}'})}$ indicates that the system has time-reversal symmetry around a node without spin-rotational symmetry, belonging to the symplectic class. A system possessing a time-reversal operator of this kind exhibits WAL. In contrast, the presence of internode scattering can induce a crossover from the symplectic to orthogonal class, leading to the corresponding crossover from WAL to WL [30]. Thus, the overall quantum correction in the DSM phase is determined by the dominant scattering mechanism, which depends on the separation between the two nodes. In the $E_F \ll |E_{\mathrm{g}}|$ limit, a large separation between the nodes will suppress the internode scattering rates, and thus the WAL effect might be dominant over the WL effect. In addition, increasing the Fermi energy leads to the distortion of the Fermi surface, suppressing WAL.

In summary, we developed a quantum interference theory for anisotropic systems by solving the Bethe-Salpeter equation for the Cooperon operator, fully considering the anisotropy and Berry phase of the system. We elaborated the Cooperon ansatz and diffusion coefficients in a compact and physically intuitive form with transport relaxation times in anisotropic systems, generalizing the previous work by P. Wölfle *et al.* [57]. Furthermore, we considered systems with nontrivial Berry phase, providing a systematic quantum interference theory for both WL and WAL effects, and the crossover between them.

# Chapter 6

# Conclusion

The work in this thesis focuses on the development of rigorous frameworks for computing dc conductivity in disordered systems with an anisotropic Fermi surface. To this end, we used various theoretical approaches: the semiclassical Boltzmann transport theory and a many-body diagrammatic method. Feynman diagrams giving a major correction to dc conductivity depend on the relative strengths of characteristic length scales. Thus, we developed the two distinct diagrammatic formalisms for the semiclassical and quantum regimes, respectively.

First, we constructed a diagrammatic formalism for computing the dc conductivity of anisotropic multiband systems in the semiclassical regime. Using Feynman diagrams, we derived coupled integral equations satisfied by transport relaxation times for impurity scattering and phonon-mediated scattering, respectively. We concluded that the Boltzmann transport equation generally corresponds to the Kubo formula supplemented with the ladder vertex corrections. We believe our results are essential for the correct computation of the Boltzmann conductivity of strongly anisotropic systems, which defy a simple description based on a model with different effective masses in each direction.

Next, we studied quantum interference effects on the dc conductivity of anisotropic systems, applying the main results of the semiclassical regime. Using a Green's func-

tion method, we obtained a general Cooperon ansatz of the Bethe-Salpeter equation in anisotropic systems. We numerically calculated magnetoconductivity for each phase of few-layer black phosphorus, and found that the ratio of the magnetoconductivity to the Boltzmann conductivity is independent of direction. We believe our work is vital for estimating the effects of lattice anisotropy and band topology on weak localization and antilocalizatioin.

# Bibliography

[1] P. W. Anderson, Absence of diffusion in certain random lattices, Phys. Rev. **109**, 1492 (1958).

[2] Shinobu Hikami, Anatoly I. Larkin, and Yosuke Nagaoka, Spin-orbit interaction and magnetoresistance in the two dimensional random system, Prog. Theor. Phys. **63**, 707 (1980).

[3] Patrick A. Lee and T. V. Ramakrishnan, Disordered electronic systems, Rev. Mod. Phys. **57**, 287 (1985).

[4] S. Datta, *Electronic Transport in Mesoscopic Systems* (Cambridge University Press, Cambridge, England, 1995).

[5] E. Akkermans and G. Montambaux, *Mesoscopic Physics of Electrons and Photons* (Cambridge University Press, Cambridge, England, 2007).

[6] N. W. Ashcroft and N. D. Mermin, *Solid State Physics*, (Brooks Cole, Pacific Grove, CA, 1976).

[7] Gerald D. Mahan, *Many-particle physics*, 3rd ed. (Springer, Berlin, 2000).

[8] P. Coleman, *Introduction to Many-Body Physics* (Cambridge University Press, Cambridge, 2016).

[9] Cong Xiao, Dingping Li, and Zhongshui Ma, Unconventional thermoelectric behaviors and enhancement of figure of merit in Rashba spintronics systems, Phys. Rev. B **93**, 075150 (2016).

[10] Valentina Brosco, Lara Benfatto, Emmanuele Cappelluti, and Claudio Grimaldi, Unconventional dc Transport in Rashba Electron Gases, Phys. Rev. Lett. **116**, 166602 (2016).

[11] Cong Xiao, Dingping Li, and Zhongshui Ma, Role of band-index-dependent transport relaxation times in anomalous Hall effect, Phys. Rev. B **95**, 035426 (2017).

[12] Sanghyun Park, Seungchan Woo, E. J. Mele, and Hongki Min, Semiclassical Boltzmann transport theory for multi-Weyl semimetals, Phys. Rev. B **95**, 161113(R) (2017).

[13] Seungchan Woo, E. H. Hwang, and Hongki Min, Large negative differential transconductance in multilayer graphene: the role of intersubband scattering, 2D Mater. **4**, 025090 (2017).

[14] Sanghyun Park, Seungchan Woo, and Hongki Min, Semiclassical Boltzmann transport theory of few-layer black phosphorous in various phases, 2D Mater. **6**, 025016 (2019).

[15] A. A. Burkov, M. D. Hook, and Leon Balents, Topological nodal semimetals, Phys. Rev. B **84**, 235126 (2011).

[16] Chen Fang, Hongming Weng, Xi Dai, and Zhong Fang, Topological nodal line semimetals, Chin. Phys. B **25**, 117106 (2016).

[17] Chen Fang, Matthew J. Gilbert, Xi Dai, and B. Andrei Bernevig, Multi-Weyl Topological Semimetals Stabilized by Point Group Symmetry, Phys. Rev. Lett. **108**, 266802 (2012).

[18] Ruixiang Fei, Vy Tran, and Li Yang, Topologically protected Dirac cones in compressed bulk black phosphorus, Phys. Rev. B **91**, 195319 (2015).

[19] Alexandra Carvalho, Min Wang, Xi Zhu, Aleksandr S. Rodin, Haibin Su, and Antonio H. Castro Neto, Phosphorene: from theory to applications, Nature Reviews Materials **1**, 16061 (2016).

[20] G. Rui, S. Zdenek and P. Martin, Black Phosphorus Rediscovered: From Bulk Material to Monolayers, Angew. Chem. Int. Ed. **56**, 8052 (2017).

[21] W. Kohn and J. M. Luttinger, Quantum Theory of Electrical Transport Phenomena, Phys. Rev. **108**, 590 (1957).

[22] Tsuneya Ando, Alan B. Fowler, and Frank Stern, Electronic properties of two-dimensional systems, Rev. Mod. Phys. **54**, 437 (1982).

[23] Ferry D. K., S. M. Goodnick, and J. Bird, *Transport in Nanostructures*, 2nd ed. (Cambridge University Press, Cambridge, England. 2009).

[24] T. Kawamura and S. Das Sarma, Phonon-scattering-limited electron mobilities in $Al_x Ga_{1-x}As$/GaAs heterojunctions, Phys. Rev. B **45**, 3612 (1992).

[25] J. M. Ziman, *Electrons and Phonons* (Oxford University Press, New York, 1963).

[26] H. Bruus and K. Flesberg, *Many-body Quantum Theory in Condensed Matter Physics* (Oxford University Press, Oxford, 2004).

[27] J. C. Ward, An Identity in Quantum Electrodynamics, Phys. Rev. **78**, 182 (1950).

[28] S. Engelsberg and J. R. Schrieffer, Coupled Electron-Phonon System, Phys. Rev. **131**, 993 (1963).

[29] E. McCann, K. Kechedzhi, Vladimir I. Fal'ko, H. Suzuura, T. Ando, and B. L. Altshuler, Weak-Localization Magnetoresistance and Valley Symmetry in Graphene, Phys. Rev. Lett. **97**, 146805 (2006).

[30] Hidekatsu Suzuura and Tsuneya Ando, Crossover from Symplectic to Orthogonal Class in a Two-Dimensional Honeycomb Lattice, Phys. Rev. Lett. **89**, 266603 (2002).

[31] Hai-Zhou Lu and Shun-Qing Shen, Weak antilocalization and localization in disordered and interacting Weyl semimetals, Phys. Rev. B **92**, 035203 (2015).

[32] Wei Chen, Hai-Zhou Lu, and Oded Zilberberg, Weak Localization and Antilocalization in Nodal-Line Semimetals: Dimensionality and Topological Effects, Phys. Rev. Lett. **122**, 196603 (2019).

[33] A. S. Rodin, A. Carvalho, and A. H. Castro Neto, Strain-induced gap modification in black phosphorus, Phys. Rev. Lett. **112**, 176801 (2014).

[34] A. N. Rudenko and M. I. Katsnelson, Quasiparticle band structure and tight-binding model for single- and bilayer black phosphorus, Phys. Rev. B **89**, 201408 (2014).

[35] Qihang Liu, Xiuwen Zhang, L. B. Abdalla, Adalberto Fazzio, and Alex Zunger, Switching a normal insulator into a topological insulator via electric field with application to phosphorene, Nano Lett. **15**, 1222 (2015).

[36] Shengjun Yuan, A. N. Rudenko, and M. I. Katsnelson, Transport and optical properties of single- and bilayer black phosphorus with defects, Phys. Rev. B **91**, 115436 (2015).

[37] Jimin Kim, Seung Su Baik, Sae Hee Ryu, Yeongsup Sohn, Soohyung Park, Byeong-Gyu Park, Jonathan Denlinger, Yeonjin Yi, Hyoung Joon Choi, and

Keun Su Kim, Observation of tunable band gap and anisotropic Dirac semimetal state in black phosphorus, Science **349**, 723 (2015).

[38] J. M. Pereira, Jr. and M. I. Katsnelson, Landau levels of single-layer and bilayer phosphorene, Phys. Rev. B **92**, 075437 (2015).

[39] Seung Su Baik, Keun Su Kim, Yeonjin Yi, and Hyoung Joon Choi, Emergence of two-dimensional massless Dirac fermions, chiral pseudospins, and Berry's Phase in potassium doped few-layer black phosphorus, Nano Lett. **15** 7788 (2015).

[40] P. Adroguer, D. Carpentier, G. Montambaux, and E. Orignac, Diffusion of Dirac fermions across a topological merging transition in two dimensions, Phys. Rev. B **93**, 125113 (2016).

[41] Shengjun Yuan, Edo van Veen, Mikhail I. Katsnelson, and Rafael Roldán, Quantum Hall effect and semiconductor-to-semimetal transition in biased black phosphorus, Phys. Rev. B **93**, 245433 (2016).

[42] Hyeonjin Doh and Hyoung Joon Choi, Dirac-semimetal phase diagram of two-dimensional black phosphorus, 2D Mater. **4**, 025071 (2017).

[43] Jimin Kim, Seung Su Baik, Sung Won Jung, Yeongsup Sohn, Sae Hee Ryu, Hyoung Joon Choi, Bohm-Jung Yang, and Keun Su Kim, Two-dimensional Dirac fermions protected by space-time inversion symmetry in black phosphorus, Phys. Rev. Lett. **119**, 226801 (2017).

[44] Jiho Jang, Seongjin Ahn, and Hongki Min, Optical conductivity of black phosphorus with a tunable electronic structure, 2D Mater. **6** ,025029 (2019).

[45] Likai Li, Yijun Yu, Guo Jun Ye, Qingqin Ge, Xuedong Ou, Hua Wu, Donglai Feng, Xian Hui Chen, and Yuanbo Zhang, Black phosphorus field-effect transistors, Nat. Nanotechnol. **9**, 372 (2014).

[46] Fengnian Xia, Han Wang, and Yichen Jia, Rediscovering black phosphorus as an anisotropic layered material for optoelectronics and electronics, Nat. Commun. **5** 4458 (2014).

[47] Vy Tran, Ryan Soklaski, Yufeng Liang, and Li Yang, Layer-controlled band gap and anisotropic excitons in few-layer black phosphorus, Phys. Rev. B **89**, 235319 (2014).

[48] Jingsi Qiao, Xianghua Kong, Zhi-Xin Hu, Feng Yang, and Wei Ji, High-mobility transport anisotropy and linear dichroism in few-layer black phosphorus, Nat. Commun. **5**, 4475 (2014).

[49] Z. J. Xiang, G. J. Ye, C. Shang, B. Lei, N. Z. Wang, K. S. Yang, D. Y. Liu, F. B. Meng, X. G. Luo, L. J. Zou, Z. Sun, Y. Zhang, and X. H. Chen, Pressure-induced electronic transition in black phosphorus, Phys. Rev. Lett. **115**, 186403 (2015).

[50] Yuchen Du, Adam T Neal, Hong Zhou, and Peide D Ye, Weak localization in few-layer black phosphorus, 2D Mater. **3**, 024003 (2016).

[51] Yanmeng Shi, Nathaniel Gillgren, Timothy Espiritu, Son Tran, Jiawei Yang, Kenji Watanabe, Takahashi Taniguchi, and Chun Ning Lau, Weak localization and electron–electron interactions in few layer black phosphorus devices, 2D Mater. **3**, 034003 (2016).

[52] N. Hemsworth, V. Tayari, F. Telesio, S. Xiang, S. Roddaro, M. Caporali, A. Ienco, M. Serrano-Ruiz, M. Peruzzini, G. Gervais, T. Szkopek, and S. Heun, Dephasing in strongly anisotropic black phosphorus, Phys. Rev. B **94**, 245404 (2016).

[53] Chun-Hong Li, Yu-Jia Long, Ling-Xiao Zhao, Lei Shan, Zhi-An Ren, Jian-Zhou Zhao, Hong-Ming Weng, Xi Dai, Zhong Fang, Cong Ren, and Gen-Fu Chen,

Pressure-induced topological phase transitions and strongly anisotropic magnetoresistance in bulk black phosphorus, Phys. Rev. B **95**, 125417 (2017).

[54] Petra Dietl, Frédéric Piéchon, and Gilles Montambaux, New magnetic field dependence of Landau levels in a graphenelike structure, Phys. Rev. Lett. **100**, 236405 (2008).

[55] Hai-Zhou Lu and Shun-Qing Shen, Quantum transport in topological semimetals under magnetic fields, Front. Phys. **12**, 127201 (2017).

[56] Freeman J. Dyson, Statistical Theory of the Energy Levels of Complex Systems. 1, J. Math. Phys. (N.Y.) **3**, 140 (1962).

[57] P. Wölfle and R. N. Bhatt, Electron localization in anisotropic systems, Phys. Rev. B **30**, 3542 (1984).

# 초 록

불순물이 있는 계에서의 전하 수송은 응집 물질 물리의 중요한 연구 주제 중 하나이다. 등방성 에너지 분산을 가지는 계에서는 볼츠만 수송 이론과 다이어그램 접근법 (diagrammatic approach) 등을 통해 전기 전도도를 계산하는 방법이 잘 구축되어 있다. 이와 달리 비등방성 에너지 분산을 가지는 계의 전기 전도도를 정확히 계산하는 것은 까다로운 문제이다. 이에 본 논문에서는 다이어그램 접근법을 이용해 비등방성계의 수송 성질을 연구하기 위한 엄밀한 계산 체계를 고안하였다.

첫째로 비등방성 다층띠를 가지는 계에서의 고전적인 수송 이론을 구축하였다. 먼저 볼츠만 수송 이론을 일반화하였고, 그 다음 사다리 다이어그램이 전기 전도도에 주는 보정을 계산하여 수송 풀림 시간 (transport relaxation time) 이 만족하는 관계식을 얻었다. 이를 통해 두 이론이 일반적으로 같은 결과를 준다는 것을 보였다.

또한 양자 영역에서의 독특한 수송 현상인 약한 국소화에 대해 연구하였다. 먼저 비등방성계에서 베테-샐피터 (Bethe-Salpeter) 방정식의 쿠페론 (Cooperon) 해를 유도하였고, 이를 이용해 다층 흑린의 여러 상 (phase) 에서 약한 국소화를 연구하였다. 그 결과, 다른 상들과 달리 반-디락 준금속 전이점 (semi-Dirac transition point) 에서 자기 전도도의 자기장 의존성이 독특한 멱법칙을 따름을 확인하였다. 또한 자기 전도도와 볼츠만 전도도의 비율이 방향 의존성을 가지지 않음을 증명하였다.

# ACKNOWLEGEMENT